An International Journal of Optimization and Control: Theories & Applications
ISSN: 2146-0957 eISSN: 2146-5703
Vol.16, No.5, pp.1787-1818 (2026)
https://doi.org/10.36922/IJOCTA026240119

RESEARCH ARTICLE

DDPG-based adaptive energy management of a PV–wind–BESS cold-ironing DC microgrid for sustainable port electrification

Mohab M. Eweda*, Rana M. Ahmed, Mona I. Abdelkader, and Ahmed K. Abdelsalam

Department of Electrical and Control Engineering, College of Engineering and Technology, Arab Academy for Science, Technology and Maritime Transport, Alexandria, Alexandria Governorate, Egypt

mohabeweda@live.com; rana-maher@aast.edu; engmonaibrahim@aast.edu; ahmed.kadry@aast.edu

ARTICLE INFO

Article history:
Received: June 14, 2026
Revised: July 29, 2026
Accepted: August 3, 2026
Published Online: August 12, 2026

Keywords:
Cold ironing
Photovoltaic–wind–battery energy storage system
Deep deterministic policy gradient
Energy management system
Direct current microgrid
Battery energy storage system
Port electrification

ABSTRACT

Cold ironing reduces ship emissions in ports, but reliable renewable-based shore power requires effective energy management. This paper presents a deep deterministic policy gradient (DDPG)-based energy management system (EMS) for a photovoltaic (PV)–wind–battery energy storage system (BESS) cold-ironing direct current (DC) microgrid designed to supply renewable shore power to berthed ships. The proposed system consists of 2 MW PV arrays, a 1 MW permanent magnet synchronous generator wind turbine, a 1 MWh BESS, a regulated 1,000 V DC bus, a shore-side power conversion unit, and a backup grid interface activated only in case of failure of the standalone renewable energy sources/BESS system. A complete dynamic model was developed in MATLAB/Simulink to evaluate system performance under normal operation, renewable-power shortage, excess-generation conditions, and realistic Alexandria Port meteorological data. A conventional rule-based EMS was first implemented as a baseline controller to coordinate renewable generation, battery charging/discharging, PV power limitation, and DC-bus regulation. Then, a DDPG-based EMS was developed to generate continuous battery-control actions and supervise PV and wind operating conditions under variable renewable generation. The results show that the proposed PV–wind–BESS system maintained the DC-bus voltage close to its 1,000 V reference while reliably supplying the cold-ironing load. Compared with the conventional EMS, the DDPG-based EMS provided smoother battery response, improved renewable-source coordination, and reduced voltage fluctuations during critical shortage and excess-generation cases. The Alexandria Port case study further validates the performance of the proposed DDPG-based EMS under realistic operating conditions for renewable-powered cold ironing in Mediterranean and North-African coastal ports.

1. Introduction

The maritime transportation sector plays a vital role in global trade but remains a significant contributor to greenhouse gas emissions and local air pollution. While international regulations have primarily focused on reducing emissions during navigation, emissions from ships while berthed at ports have become an increasing environmental concern, particularly in densely populated coastal cities. During berthing, ships continue operating auxiliary diesel generators to supply onboard hoteling loads, resulting in continuous emissions of carbon dioxide (CO_2), nitrogen oxides (NO_X), sulfur oxides (SO_X), particulate matter (PM), and noise. Consequently, port electrification through cold ironing, also referred to as shore power or onshore power supply, has

*Corresponding Author

emerged as one of the most effective strategies for eliminating emissions from berthed vessels by transferring onboard electrical demand to shore-based power systems.[1,2]

The environmental benefits of cold ironing, however, depend strongly on the electricity source supplying the port. When shore power is obtained from fossil-fuel-dominated utility grids, emissions are shifted from the port to the power generation sector rather than eliminated. Integrating renewable energy resources with shore power therefore represents a more sustainable solution by simultaneously reducing local air pollution and the overall carbon footprint of maritime operations.[3,4] Hybrid photovoltaic (PV)–wind–battery energy storage system (BESS) microgrids have consequently attracted increasing attention because they combine the complementary characteristics of solar and wind generation while using battery storage to compensate for the intermittency of renewable energy sources (RES).

Although renewable-powered microgrids have been extensively investigated, applying them to cold-ironing systems introduces several operational challenges distinct from those encountered in conventional microgrids. Unlike residential or commercial microgrids, shore-power systems must continuously supply large electrical loads without interruption throughout the berthing period. In addition, ship connection and disconnection events may introduce rapid variations in power demand, while the direct current (DC) bus must remain tightly regulated to ensure reliable operation of the power electronic conversion stages supplying the vessel. At the same time, the energy management system (EMS) must coordinate multiple RES, battery charging and discharging, renewable power curtailment during surplus generation, and emergency grid support under severe renewable energy deficits. These simultaneous control objectives make cold-ironing microgrids a particularly demanding application for real-time energy management.[5-9]

Conventional EMS strategies are commonly based on predefined rules, threshold logic, and proportional-integral (PI) controllers because of their simplicity and ease of implementation. However, their performance depends heavily on manually designed operating rules and fixed switching thresholds, which may become suboptimal under rapidly changing renewable generation and load conditions.[10-12] As renewable penetration increases, the nonlinear interactions among PV generation, wind generation, battery dynamics, and DC-bus voltage regulation become increasingly difficult to manage using deterministic control strategies alone.

Recent advances in artificial intelligence have encouraged the application of reinforcement learning (RL) and deep reinforcement learning (DRL) to energy management problems. Unlike conventional controllers, DRL enables an agent to continuously improve its control policy through interaction with the operating environment without requiring an explicit mathematical optimization model. Among DRL algorithms, deep deterministic policy gradient (DDPG) is particularly suitable for renewable energy management because it directly generates continuous control actions, making it well suited for battery charging/discharging control, renewable power coordination, and converter-level power regulation.[13-20]

Despite this progress, most existing DRL-based studies have focused on general microgrid scheduling, economic dispatch, or battery management. Comparatively fewer studies have investigated intelligent energy management for renewable-powered cold-ironing DC microgrids, where uninterrupted ship supply, stringent DC-bus voltage regulation, coordinated operation of multiple RES, and battery protection must be achieved simultaneously. Furthermore, most published cold-ironing case studies have concentrated on European, North American, and East Asian ports, while relatively limited attention has been given to Mediterranean and North African ports, whose renewable resource characteristics, infrastructure maturity, and electrification requirements differ from those previously reported. Rather than proposing a fundamentally different control problem, these regional characteristics motivate the evaluation of advanced EMS strategies under operating conditions representative of emerging port electrification projects.

To address these challenges, this study proposes a DDPG-based adaptive EMS for a PV–wind–BESS cold-ironing DC microgrid supplying shore power to berthed ships. A detailed MATLAB/Simulink dynamic model was developed to compare the proposed DDPG-based controller with a conventional rule-based EMS under identical operating conditions, including normal operation, renewable generation shortages, excess renewable generation, and realistic meteorological data for Alexandria Port, Egypt.

The main contributions of this work are

summarized as follows:

(i) Development of a detailed dynamic model of a renewable-powered PV–wind–BESS cold-ironing DC microgrid incorporating PV generation, wind generation, battery energy storage, a regulated DC bus, shore-side power conversion, and emergency grid backup.
(ii) Design and implementation of a DDPG-based adaptive EMS capable of generating continuous battery control actions while coordinating renewable generation and DC-bus voltage regulation.
(iii) Comprehensive comparison between the proposed DDPG-based EMS and a conventional rule-based EMS under identical operating scenarios to evaluate their dynamic performance.
(iv) Validation of the proposed framework using realistic renewable resource profiles for Alexandria Port to assess its applicability to Mediterranean and North African port electrification.

The remainder of this paper is organized as follows: Section 2 presents the proposed PV–wind–BESS cold-ironing microgrid and its mathematical modeling. Section 3 describes the conventional and DDPG-based energy management strategies. Section 4 presents the simulation results and comparative performance evaluation. Section 5 discusses the obtained results, comparative performance, and practical implications of the proposed DDPG-based EMS. Finally, Section 6 concludes the paper and outlines future research directions.

2. Proposed system

2.1. Proposed system architecture

The proposed system is a renewable-powered cold-ironing DC microgrid designed to supply shore-side electrical power to berthed ships. The system consists of two PV arrays, a wind energy conversion system, a BESS, a common DC bus, a shore-side cold-ironing conversion unit, and an emergency grid backup interface. The general configuration of the proposed system is shown in **Figure 1**. The RES and BESS are connected to a regulated 1,000 V DC bus through dedicated power electronic converters, while the cold-ironing unit converts the available DC-side energy into the required AC voltage and frequency for the ship-side load.

The common DC-bus architecture is selected because it provides a suitable interface for integrating renewable generation, battery storage, and converter-based loads. In this configuration, the DC bus acts as the main power exchange node between the PV arrays, the wind turbine,

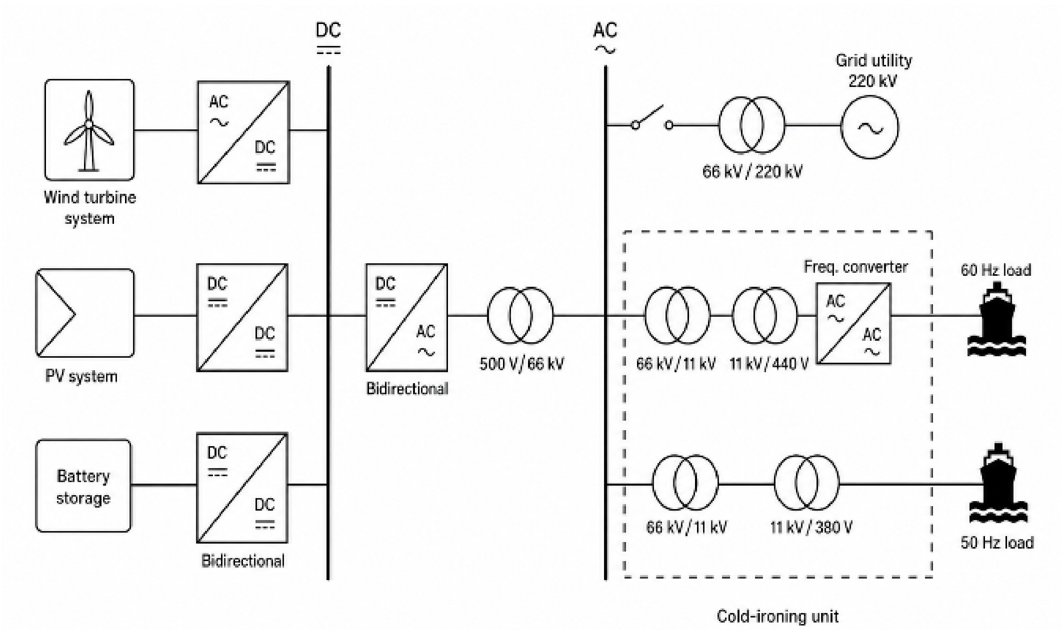

Figure 1. Proposed PV–wind–BESS cold-ironing DC microgrid with common DC bus, shore-side conversion unit, and emergency grid backup interface
Abbreviations: AC: Alternating current; BESS: Battery energy storage system; DC: Direct current; Freq.: Frequency; PV: Photovoltaic.

the BESS, and the cold-ironing unit. The PV subsystem supplies solar power through DC–DC boost converters, while the wind turbine subsystem supplies power through a generator-side power electronic interface. The BESS is connected through a bidirectional DC–DC converter to absorb surplus power or support the DC bus during periods of renewable generation shortage. The emergency grid interface is included only as a backup supply path and is not used for normal power sharing.

The total renewable power supplied to the DC bus is obtained from the PV and wind contributions as:

$$P_{\mathrm{RES}} = P_{\mathrm{PV1}} + P_{\mathrm{PV2}} + P_{\mathrm{WT}} \tag{1}$$

where P_{PV1} and P_{PV2} are the powers of the two PV arrays, and P_{WT} is the wind turbine output power. This power is used to supply the cold-ironing load, charge or discharge the BESS, and reduce the need for emergency grid backup. The detailed coordination logic is presented later in Section 3.

2.2. Photovoltaic subsystem modeling

The PV subsystem consists of two independently controlled PV arrays. PV Array 1 represents the main solar generation unit and is rated at approximately 1.5 MW, while PV Array 2 is rated at approximately 0.5 MW. Each PV array is connected to the common DC bus through an independent DC–DC boost converter. This structure allows each array to respond separately to variations in irradiance and temperature, which is important when the two arrays are installed in different port areas or exposed to different environmental conditions.

The PV cell is represented using the single-diode model, which is widely used to describe the nonlinear current–voltage characteristics of PV cells under varying irradiance and temperature conditions.[21,22] The equivalent circuit includes a photocurrent source, a diode, a series resistance, and a shunt resistance, as shown in **Figure 2**. The PV output current is expressed as:[23]

$$I_{PV} = I_{ph} - I_0\left[\exp\left(\frac{V_{PV} + I_{PV}R_s}{aV_t}\right) - 1\right] - \frac{V_{\mathrm{PV}} + I_{\mathrm{PV}}R_s}{R_{sh}} \tag{2}$$

where I_{PV} is the PV output current, I_{ph} is the photocurrent, I_0 is the diode reverse saturation current, V_{PV} is the PV terminal voltage, R_s and R_{sh} are the series and shunt resistances, a is the diode ideality factor, and V_t is the thermal voltage. The PV cell is represented by the widely adopted single-diode equivalent circuit model shown in **Figure 2**.[21]

For array-level modeling, the PV voltage and current are scaled according to the number of series-connected modules and parallel strings:[24]

$$V_{\mathrm{array}} = N_s V_{\mathrm{module}} \tag{3}$$

$$I_{\mathrm{array}} = N_p I_{\mathrm{module}} \tag{4}$$

where N_s is the number of modules connected in series, and N_p is the number of parallel strings. In the proposed system, PV Array 1 is configured using 15 series-connected modules per string and 282 parallel strings, while PV Array 2 is configured using 14 series-connected modules per

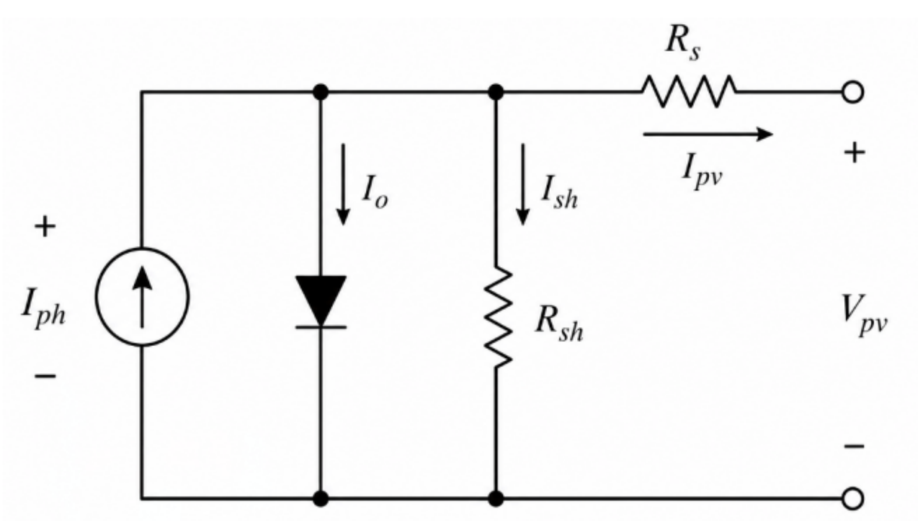

Figure 2. Single-diode equivalent circuit used for photovoltaic cell modeling

string and 122 parallel strings. The combined installed PV capacity is approximately 2 MW.

The PV array characteristics are evaluated under different irradiance and temperature levels, as shown in **Figure 3**. The curves confirm that irradiance mainly affects the PV output current and generated power, while temperature mainly affects the output voltage and shifts the maximum power point. Therefore, maximum power point tracking (MPPT) is required to maintain efficient PV operation under changing weather conditions.

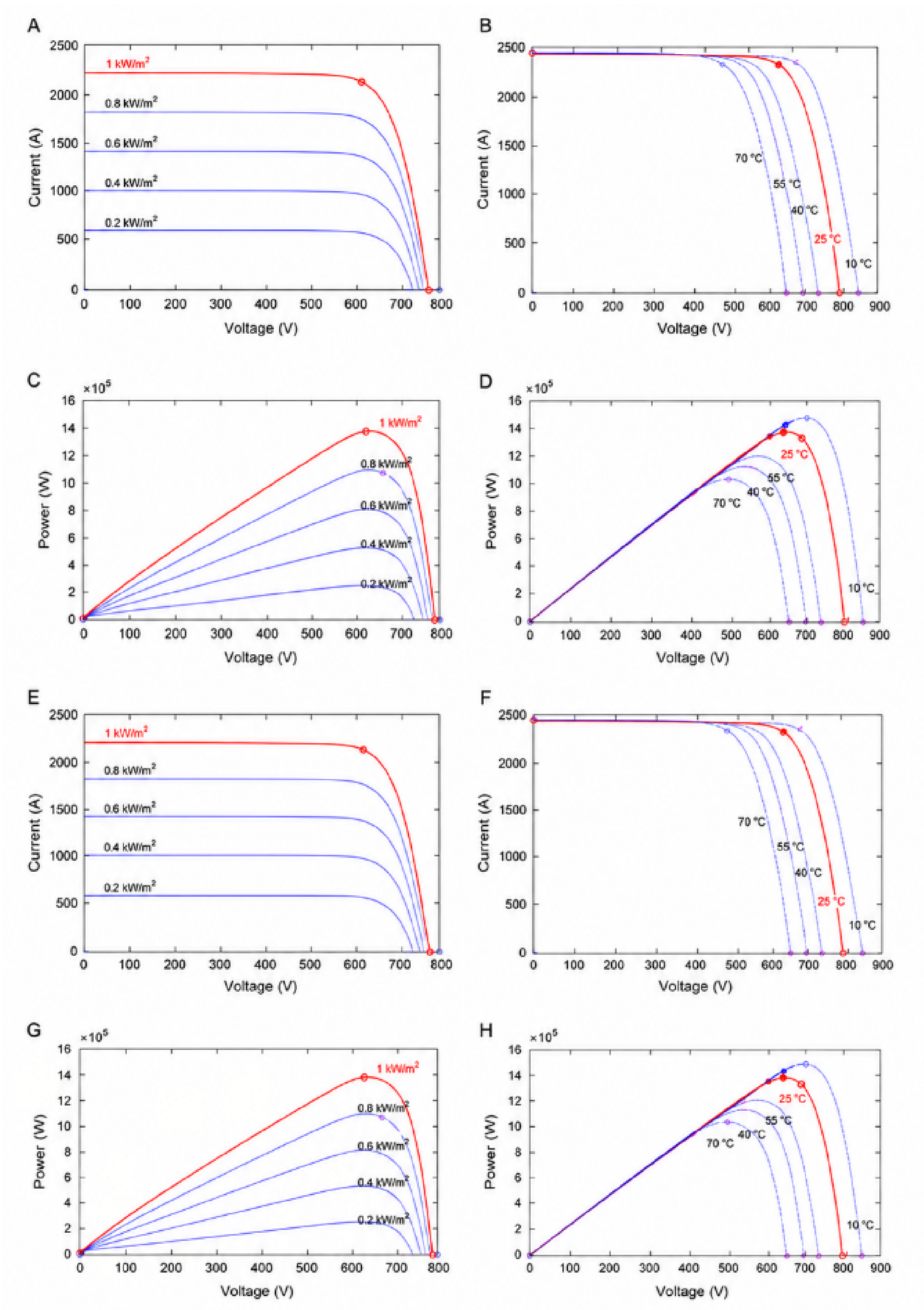

Figure 3. Current (I)–voltage (V) and power (P)–V characteristics of the two photovoltaic (PV) arrays under different irradiance and temperature conditions. (A) I–V and (B) P–V of PV Array 1 under irradiance variation. (C) I–V and (D) P–V of PV Array 1 under temperature variation. (E) I–V and (F) P–V of PV Array 2 under irradiance variation. (G) I–V and (H) P–V of PV Array 2 under temperature variation.

Each PV array is controlled using a perturb-and-observe (P&O) MPPT algorithm. The P&O method is selected because it is simple, practical, and requires only PV voltage and current measurements.[25] The instantaneous PV power is calculated as:

$$P_{\mathrm{PV}} = V_{\mathrm{PV}} \times I_{\mathrm{PV}} \tag{5}$$

The algorithm compares changes in PV power and PV voltage and updates the boost-converter duty cycle accordingly. For the ideal boost converter, the voltage conversion relationship is:[26]

$$V_{\mathrm{dc}} = \frac{V_{\mathrm{PV}}}{1-D} \tag{6}$$

where V_{dc} is the DC-bus voltage, and D is the boost-converter duty cycle. In the proposed system, the PV converters raise the PV-side voltage to the common 1,000 V DC-bus level. The complete Simulink implementation of the 2 MW PV subsystem is shown in **Figure 4**.

2.3. Wind energy subsystem modeling

The wind energy subsystem consists of a 1 MW horizontal-axis wind turbine coupled to a permanent magnet synchronous generator (PMSG). The PMSG is selected because it is suitable for variable-speed wind energy conversion systems and offers high efficiency, self-excitation, and reduced maintenance requirements compared with externally excited generator structures.[27] The variable-frequency AC output of the PMSG is converted and regulated through a power electronic interface before being connected to the common DC bus.

The aerodynamic power available in the wind is proportional to the cube of the wind speed and is expressed as:[28]

$$P_{\mathrm{w}} = \frac{1}{2}\rho A v_{\mathrm{w}}^{3} \tag{7}$$

where ρ is the air density, A is the swept area of the rotor, and v_w is the wind speed. The swept area is calculated as:

$$A = \pi R^{2} \tag{8}$$

where R is the turbine rotor radius. The mechanical power extracted by the turbine is lower than the total available wind power and depends on the power coefficient (C_p):

$$P_{\mathrm{m}} = \frac{1}{2}\rho A C_{p}(\lambda,\beta) v_{\mathrm{w}}^{3}\eta_{\mathrm{t}} \tag{9}$$

where P_{m} is the extracted mechanical power, C_{p} is the power coefficient, λ is the tip-speed ratio

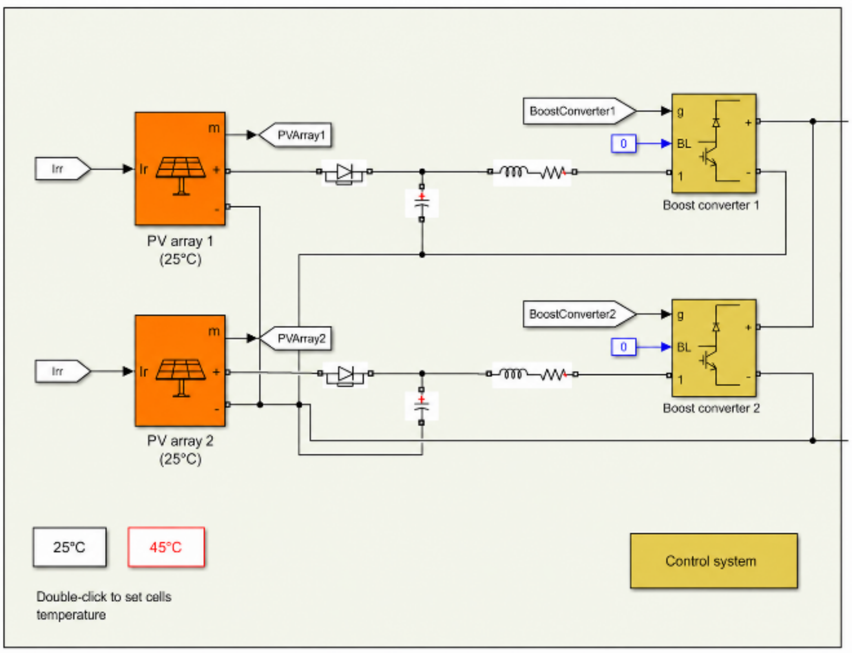

Figure 4. MATLAB/Simulink implementation of the 2 MW photovoltaic (PV) subsystem with two independently controlled PV arrays, direct current (DC)–DC boost converters, and centralized control interface

(TSR), β is the blade pitch angle, and η_t is the turbine efficiency. For the fixed-pitch turbine considered in this study, the control objective is to maintain operation near the optimum TSR. The TSR is defined as:

$$\lambda = \frac{\omega_t R}{v_w} \tag{10}$$

where ω_t is the turbine angular speed. This relationship shows that, for each wind speed, there is an optimum rotor speed that maximizes extracted power.

The wind turbine power–speed characteristics are shown in **Figure 5**. For each wind speed, the turbine reaches a maximum power point at a specific rotor speed. This behavior justifies the use of a TSR-based MPPT strategy to regulate the generator operating point and extract the available wind power efficiently.[29]

The PMSG output voltage and frequency vary with turbine speed. Therefore, a full-scale power electronic converter is required to connect the generator to the DC bus. In PMSG-based wind energy conversion systems, the AC–DC interface may be implemented using a diode-bridge rectifier followed by a DC–DC converter or using an active pulse-width modulation (PWM) rectifier. The PWM rectifier provides higher controllability, although it increases cost and control complexity.[30] In this work, the wind subsystem is represented through a controlled power electronic interface that enables variable-speed operation and DC-link compatibility. The MATLAB/Simulink implementation of the wind subsystem is shown in **Figure 6**.

2.4. Battery energy storage system

The BESS is used as the main energy-buffering element in the proposed cold-ironing microgrid. It absorbs surplus renewable power when PV and wind generation exceed cold-ironing demand and discharges when renewable generation is insufficient. This function is essential for maintaining the DC bus power balance and improving the reliability of the renewable-based shore-power supply.

The nominal energy capacity of the battery is calculated using:

$$E_{bat} = \frac{V_{bat} C_{bat}}{1000} \tag{11}$$

where E_{bat} is the nominal battery energy capacity in kWh, V_{bat} is the nominal battery voltage, and C_{bat} is the rated ampere-hour capacity. In the proposed system, the BESS is modeled as a high-voltage battery bank connected to the common DC bus through a bidirectional DC–DC converter. The main monitored variables are battery voltage, current, power, and state of charge. Simscape battery modeling is used to

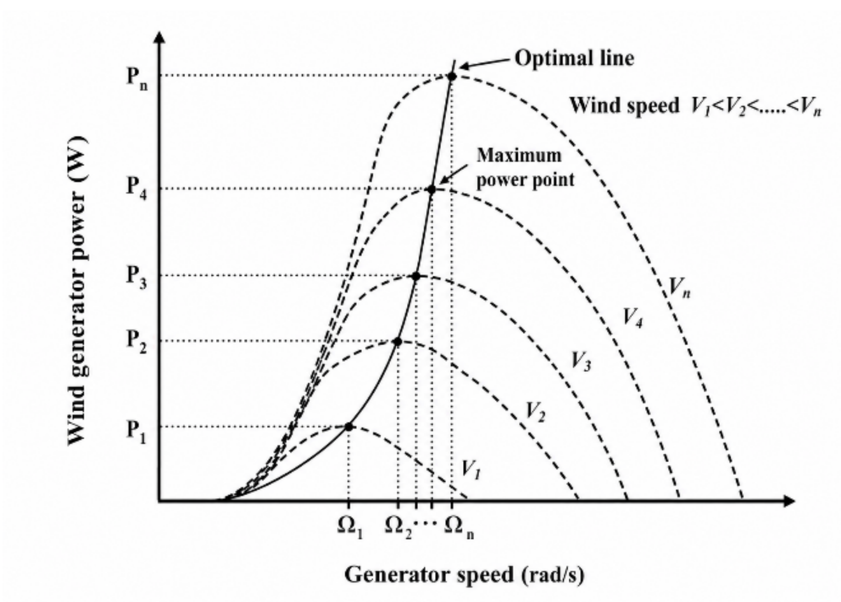

Figure 5. Power–speed characteristics of the proposed 1 MW permanent magnet synchronous generator wind turbine under different wind-speed conditions

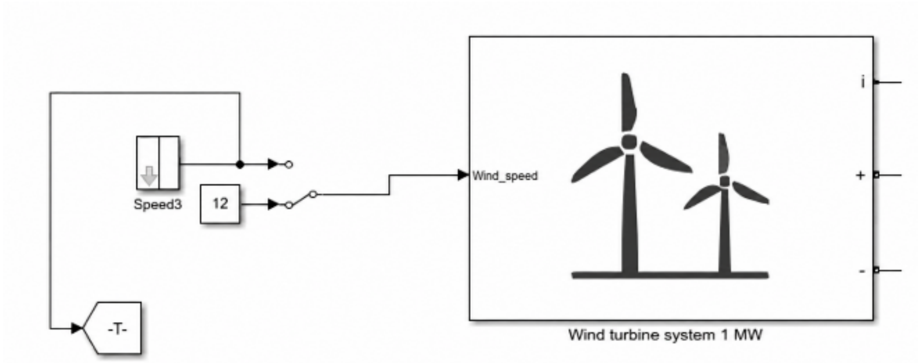

Figure 6. MATLAB/Simulink implementation of the 1 MW permanent magnet synchronous generator wind turbine subsystem with wind-speed input and power output interface

represent the electrical behavior of the battery and monitor the state of charge (SOC) during simulation.[31]

The instantaneous battery power is calculated as:

$$P_{\mathrm{bat}} = V_{\mathrm{bat}} \times I_{\mathrm{bat}} \tag{12}$$

where P_{bat} is the battery power, V_{bat} is the battery terminal voltage, and I_{bat} is the battery current. In this study, positive battery power represents discharge from the battery to the DC bus, while negative battery power represents battery charging. The battery SOC is calculated using the Coulomb-counting principle:[32]

$$SOC(t) = SOC_0 - \frac{1}{3600C_{\mathrm{bat}}}\int_0^t I_{\mathrm{bat}}(\tau)\,d\tau \tag{13}$$

where SOC_0 is the initial state of charge, and C_{bat} is the rated battery capacity in ampere-hours. The sign of I_{bat} depends on the current-direction convention used in the simulation model.

Because the nominal battery voltage is lower than the common DC-bus voltage, a bidirectional DC–DC converter is required. During discharge, the converter operates in boost mode to transfer power from the battery to the DC bus. The ideal boost duty cycle is expressed as:[33]

$$D_{\mathrm{boost}} = 1 - \frac{V_{\mathrm{bat}}}{V_{\mathrm{dc}}} \tag{14}$$

During charging, the converter operates in buck mode to transfer power from the DC bus to the battery, and the ideal buck relationship is:[34]

$$V_{\mathrm{bat}} = D_{\mathrm{buck}} \times V_{\mathrm{dc}} \tag{15}$$

The bidirectional converter therefore enables controlled charging and discharging in accordance with the EMS command. The Simulink implementation of the BESS subsystem is shown in **Figure 7**.

2.5. Cold-ironing conversion unit and ship load

The cold-ironing unit is the final power-conditioning interface between the proposed hybrid renewable DC microgrid and the berthed ship load. Practical shore-to-ship power systems require electrical conditioning because ships may require different voltage and frequency levels depending on vessel type, onboard distribution system, and operating region. High-voltage shore connection systems also require proper transformers, converters, protection devices, monitoring, and control interfaces to ensure a safe and compatible ship-side supply.[35]

In this study, the cold-ironing unit was modeled as an AC/DC/AC power conversion stage. The converter structure includes an input interface, a transformer or isolation stage, a rectifier, a DC-link capacitor, an inverter, a PWM generator, an output filter, root-mean square (RMS) measurement blocks, and a three-phase ship-side load. The general configuration is shown in **Figure 8**.

The active-power balance across the cold-ironing converter can be expressed as:

$$P_{\mathrm{in}} = P_{\mathrm{load}} + P_{\mathrm{loss}} \tag{16}$$

where P_{in} is the input power to the cold-ironing conversion unit, P_{load} is the active power delivered to the ship load, and P_{loss} represents converter and filter losses. For the ideal simulation case used in this study, converter and filter losses were neglected, and the supplied power was assumed to match the load demand.

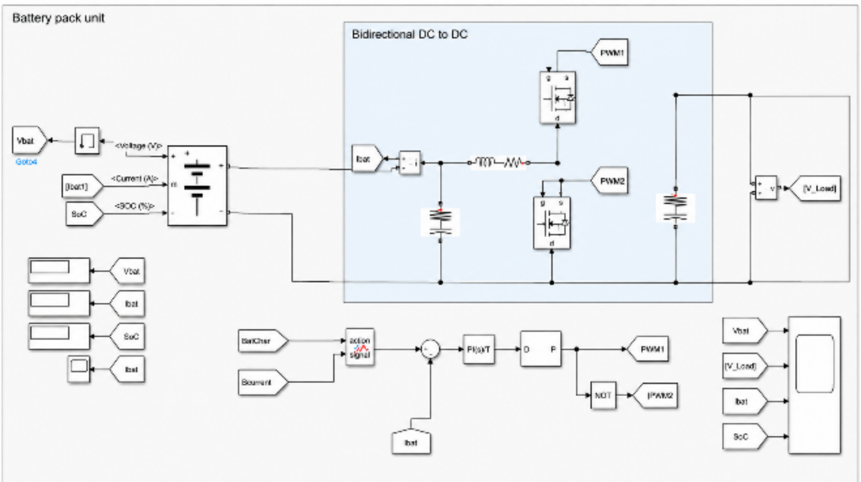

Figure 7. MATLAB/Simulink implementation of the battery energy storage system (BESS) with bidirectional direct current (DC)–DC converter and current-controlled charging/discharging interface

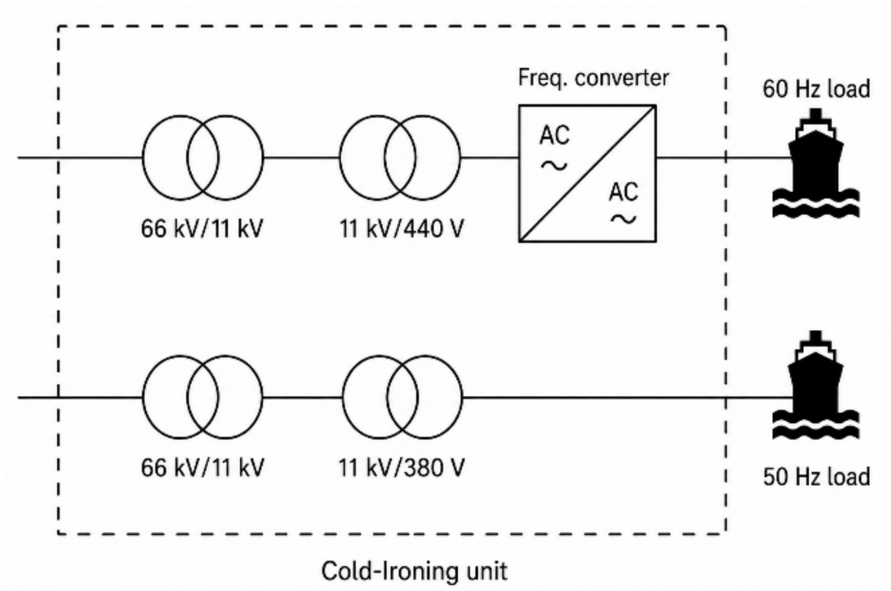

Figure 8. Cold-ironing conversion unit connecting the renewable-powered direct current (DC) microgrid to the ship-side alternating current (AC) load.
Abbreviation: Freq.: Frequency.

The ship-side load is represented as a balanced three-phase active-power load operating at unity power factor. This assumption focuses the analysis on active-power management, DC-bus voltage stability, BESS response, and EMS operation. The three-phase active power is expressed as:[36]

$$P_{\text{load}} = \sqrt{3} V_{\text{LL}} I_{\text{L}} \cos\phi \tag{17}$$

where V_{LL} is the line-to-line RMS voltage, I_{L} is the line current, and $\cos \phi$ is the power factor. Since the load is assumed to operate at unity power factor, $\cos \phi$ equals 1. The model includes two ship-side supply configurations, 440 V at 60 Hz and 380 V at 50 Hz, to represent practical shore-power requirements for different ship electrical systems. The Simulink model of the cold-ironing unit is shown in **Figure 9**.

2.6. Emergency grid backup interface

The emergency grid interface is included to improve the reliability of the shore-side power supply under critical operating conditions. Under normal operation, the cold-ironing load is supplied by the PV arrays, wind turbine, and

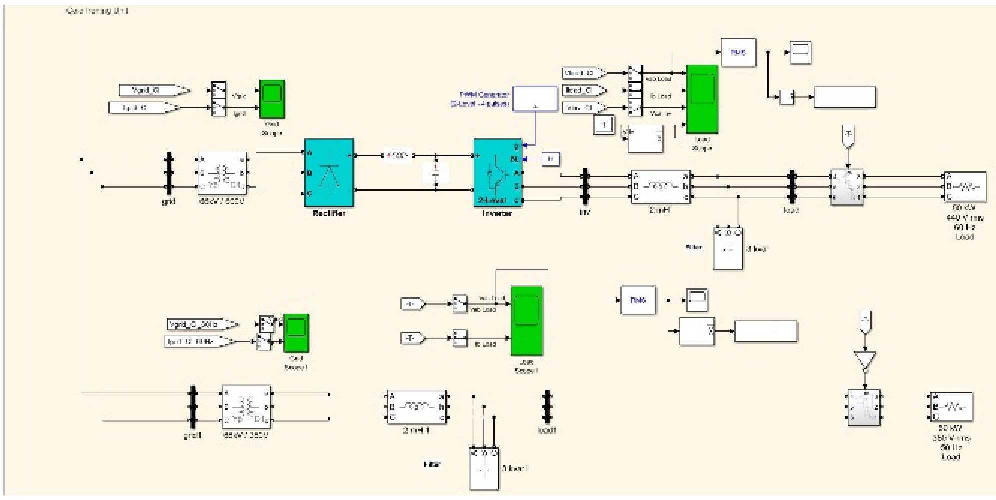

Figure 9. MATLAB/Simulink implementation of the cold-ironing conversion unit supplying the constant ship-side active-power load

BESS through the common DC bus. The utility grid is not used for normal power sharing or for exporting surplus renewable energy. Instead, it is activated only when the renewable-side system cannot maintain the cold-ironing load or when a critical system fault requires transfer to backup supply.

The backup interface follows an automatic transfer logic similar to an automatic transfer switch. During normal operation, the RES/BESS side remains connected, and the grid remains disconnected. During a renewable-side failure or critical supply shortage, the EMS isolates the renewable-side system and connects the load to the utility grid through the backup path. This structure prevents unstable parallel operation between the emergency grid path and the renewable DC microgrid while maintaining continuity of supply to the ship load. The automatic transfer logic is summarized in **Table 1**.

This section establishes the physical and mathematical modeling basis of the proposed PV–wind–BESS cold-ironing DC microgrid. The next section presents the energy management methodology used to coordinate the system components under normal, shortage, and excess renewable-generation conditions.

3. Energy management methodology

3.1 Energy management system control objectives

The EMS is developed as the supervisory control layer of the proposed PV–wind–BESS cold-ironing DC microgrid. Its main function is to coordinate power exchange among the PV arrays, wind turbine, BESS, emergency grid interface, and cold-ironing load while maintaining stable operation of the common DC bus. In the proposed system, the EMS has four main objectives: maintaining

Table 1. Emergency grid backup and automatic transfer logic

Operating condition	RES/BESS status	Grid status	Load supply source	Control action
Normal operation	Connected	Off	PV, wind, and BESS	Hybrid system supplies the cold-ironing load
Renewable-side fault or critical shortage	Disconnected	On	Utility grid	EMS isolates RES/BESS and activates grid supply

Abbreviations: BESS: Battery energy storage system; EMS: Energy management system; PV: Photovoltaic; RES: renewable energy sources.

the DC-bus voltage close to its reference value, protecting the battery from overcharging and deep discharging, maximizing renewable-energy utilization, and ensuring a continuous shore-side power supply to the berthed ship.

The EMS receives the measured PV power, wind power, battery SOC, battery voltage, load demand, DC-bus voltage, and grid-switch status. Based on these inputs, it generates the required commands for the PV operating mode, BESS bidirectional converter, RES coordination, and emergency grid switch. **Figure 10** shows the Simulink EMS control block used in the proposed cold-ironing system.

The total renewable power available at the DC bus is given by:

$$P_{\mathrm{RES}}(k) = P_{\mathrm{PV1}}(k) + P_{\mathrm{PV2}}(k) + P_{\mathrm{WT}}(k) \tag{18}$$

where P_{PV1}, P_{PV2}, and P_{WT} are the output powers of PV Array 1, PV Array 2, and the wind turbine, respectively. The power mismatch between renewable generation and the cold-ironing load is expressed as:

$$\Delta P(k) = P_{\mathrm{RES}}(k) - P_{\mathrm{load}}(k) \tag{19}$$

where P_{load} is the cold-ironing load demand. If $\Delta P > 0$, renewable generation exceeds the load demand and the system operates under surplus-power conditions. If $\Delta P < 0$, renewable generation is insufficient and the system operates under power-deficit conditions. In DC microgrids, this power mismatch directly affects the DC-bus voltage: surplus power tends to increase the bus voltage, while insufficient power decreases it.

The ideal power balance of the proposed DC microgrid can be written as:

$$P_{\mathrm{RES}}(k) + P_{\mathrm{bat}}(k) + P_{\mathrm{grid}}(k) = P_{\mathrm{load}}(k) \tag{20}$$

where P_{bat} is the battery power, and P_{grid} is the emergency grid contribution. In this study, a positive P_{bat} denotes battery discharge, while

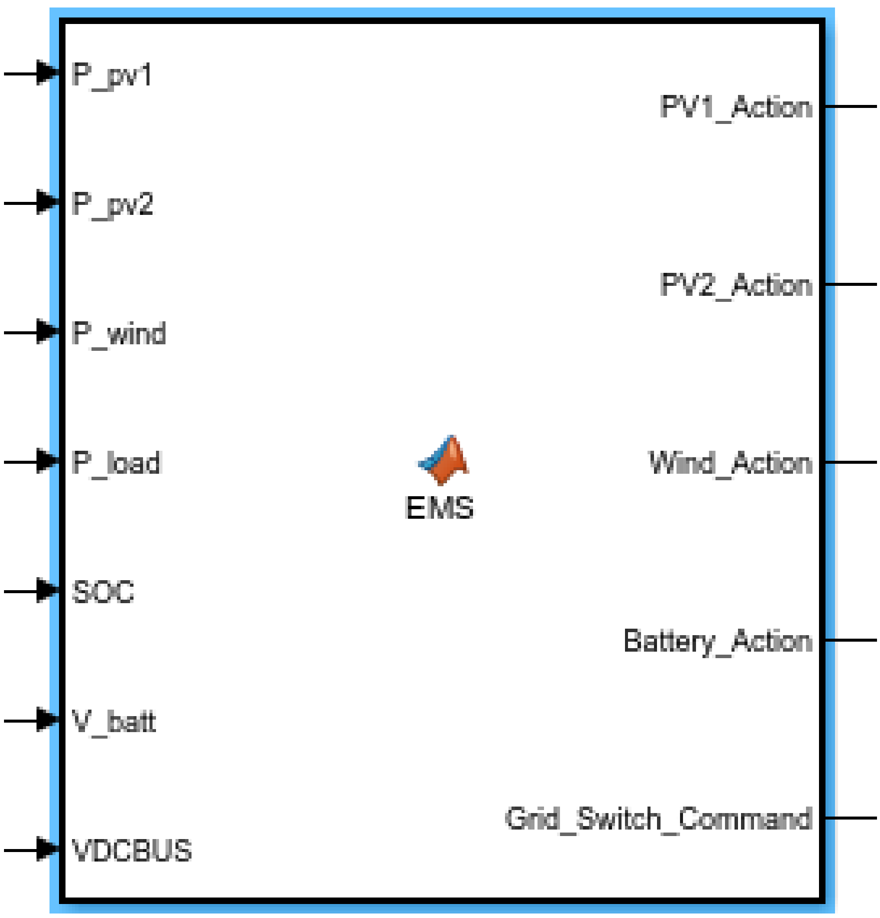

Figure 10. Simulink energy management system (EMS) control block for the proposed cold-ironing port application

a negative P_{bat} denotes battery charging. The emergency grid is not used during normal operation and is activated only when the RES/BESS side cannot maintain reliable load supply.

3.2. Conventional rule-based energy management system

A conventional EMS is implemented as a deterministic rule-based controller. Rule-based EMS strategies are widely used in hybrid renewable energy systems (HRES) because they are simple, practical, and can coordinate renewable generation, BESS operation, MPPT control, and backup supply according to predefined conditions.[37] Similar rule-based and PI-based energy management concepts have also been applied in HRES to maintain power balance and regulate voltage under variable generation conditions.[38]

In the proposed conventional EMS, RES has the priority for supplying the cold-ironing load. The BESS is then used to absorb excess renewable energy or compensate for renewable-power shortage. If the battery reaches its SOC limits, the EMS either limits the PV output power or activates the emergency grid supply. **Table 2** summarizes the main operating modes of the conventional EMS.

Figure 11 presents the overall supervisory EMS schematic. The figure shows how the EMS receives system measurements and generates control signals for PV operation, wind operation, BESS charging/discharging, DC-bus voltage support, and emergency grid switching. This structure allows the conventional EMS to coordinate the main components of the cold-ironing system using predefined logic.

The main control loops used by the conventional EMS are shown in **Figure 12**. These include the P&O-based PV MPPT controller, the TSR-based wind MPPT controller, the BESS PI controller for DC-bus voltage regulation, and the PI-based PV power-limiting controller used during excess-generation conditions.

The BESS-side PI controller is used to correct DC-bus voltage deviation by generating an additional battery current command. The voltage

Table 2. Operating modes of the conventional energy management system (EMS)

Mode	Operating condition	EMS action	RES status	BESS status
Mode 1: Balanced operation	•$P_{RES} \approx P_{load}$ •V_{dc} *close to reference*	Supply the load from PV and wind through the DC bus	PV and wind operate in MPPT mode	Idle or light support
Mode 2: Renewable surplus	•$P_{RES} > P_{load}$ •$SOC < SOC_{max}$	Use surplus renewable power to charge the battery	PV and wind remain in MPPT mode	Charging
Mode 3: Renewable surplus with high SOC	•$P_{RES} > P_{load}$ •$SOC \geq SOC_{max}$ or charging limit is reached	Activate PV power-limiting control	PV power is limited; wind remains in MPPT mode	Charging blocked/protected
Mode 4: Renewable deficit with sufficient SOC	•$P_{RES} < P_{load}$ •$SOC > SOC_{min}$	Use the BESS to compensate for the deficit	PV and wind operate in MPPT mode	Discharging
Mode 5: Renewable deficit with low SOC	•$P_{RES} < P_{load}$ •$SOC \leq SOC_{min}$	Block further discharge and activate backup supply	RES side disconnected if required	Discharge blocked

Abbreviations: BESS: Battery energy storage system; DC: Direct current; MPPT: Maximum power point tracking; PV: Photovoltaic; RES: Renewable energy sources; SOC: State of charge.

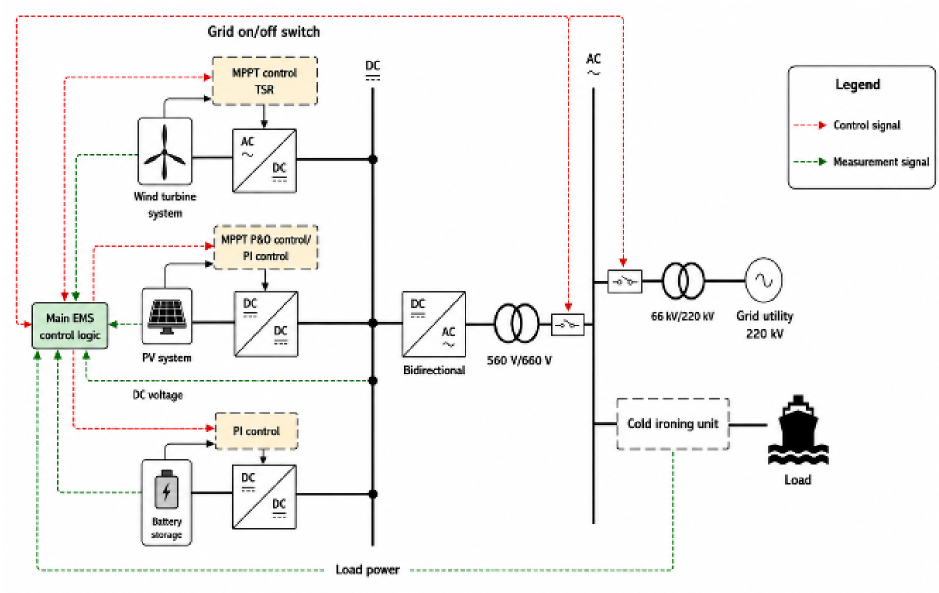

Figure 11. Supervisory EMS schematic showing measurement inputs and control commands for PV arrays, wind turbine, BESS, DC bus, cold-ironing load, and emergency grid switch.
Abbreviations: AC: Alternating current; BESS: Battery energy storage system; DC: Direct current; EMS: Energy management system; MPPT: Maximum power point tracking; P&O: Perturb and observe; PI: Proportional integral; PV: Photovoltaic; TSR: Tip speed ratio.

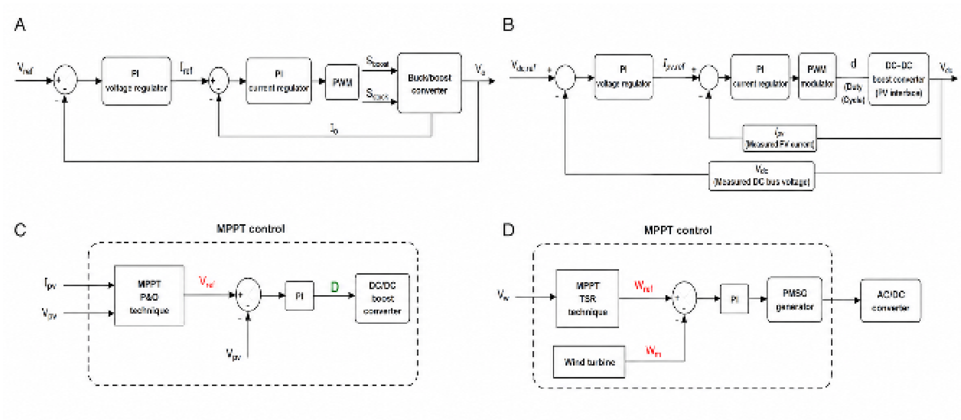

Figure 12. Main EMS control components: (a) P&O-based PV MPPT controller, (b) TSR-based wind MPPT controller, (c) BESS PI controller for DC-bus voltage regulation, and (d) PI-based PV power-limiting controller.
Abbreviations: AC: Alternating current; BESS: Battery energy storage system; DC: Direct current; EMS: Energy management system; MPPT: Maximum power point tracking; P&O: Perturb and observe; PI: Proportional integral; PMSG: Permanent magnet synchronous generator; PV: Photovoltaic; PWM: Pulse-width modulation; TSR: Tip speed ratio.

error is defined as:

$$e_v(k) = V_{\mathrm{dc,ref}} - V_{\mathrm{dc}}(k) \tag{21}$$

where $V_{\mathrm{dc,ref}}$ is the reference DC-bus voltage, and V_{dc} is the measured DC-bus voltage. The corrective current produced by the PI controller is:

$$I_{\mathrm{PI}}(k) = K_p e_v(k) + K_i \int e_v(k)\,dt \tag{22}$$

where K_p and K_i are the proportional and integral gains, respectively, of the battery-side PI controller. The proportional term improves dynamic response, while the integral term reduces steady-state error, following standard feedback-control principles.[39]

The battery current reference obtained from the EMS power command is calculated as:

$$I_{bat,\mathrm{p}}\left(k\right)=\frac{P_{\mathrm{bat}}\left(k\right)}{V_{bat}\left(k\right)} \tag{23}$$

where P^{*}_{bat} is the battery power command, and V_{bat} is the battery terminal voltage. The final current reference is obtained by combining the EMS power-based current command with the PI correction:

$$I_{\mathrm{bat}}\left(k\right)=I_{\mathrm{bat,p}}\left(k\right)+I_{\mathrm{PI}}\left(k\right) \tag{24}$$

To protect the battery and bidirectional converter, the final current command is limited using saturation:

$$I_{\mathrm{ch,max}}\leq I^{*}_{\mathrm{bat}}\left(k\right)\leq I_{\mathrm{dis,max}} \tag{25}$$

where $I_{\mathrm{ch,max}}$ and $I_{\mathrm{dis,max}}$ are the maximum allowable charging and discharging current limits, respectively. Saturation is required to prevent the control command from exceeding physical limits of the battery and converter.[40] In addition, a ramp-rate limiter is applied to reduce sudden current variations:

$$I_{\mathrm{bat,cmd}}\left(k\right)=I_{\mathrm{bat,cmd}}\left(k-1\right)+ sat\left[I^{*}_{\mathrm{bat}}\left(k\right)-I_{\mathrm{bat,cmd}}\left(k-1\right),@-\Delta I_{\mathrm{max}},\Delta I_{\mathrm{max}}\right] \tag{26}$$

where ΔI_{max} is the maximum allowed current change per sampling step. This limiter improves the smoothness of battery current and reduces converter stress during rapid changes in renewable power.[41]

3.3. Reinforcement learning formulation

Although the conventional EMS provides a practical baseline control strategy, its response is restricted by predefined thresholds and fixed operating rules. Therefore, RL is introduced to improve the adaptability of the EMS under variable renewable generation conditions. RL allows an agent to learn a control policy through repeated interaction with the environment by observing system states, applying actions, and receiving rewards that reflect the quality of each decision.[42]

The energy management problem is formulated as a Markov decision process:

$$M=\left(\mathcal{S},\mathcal{A},\mathcal{P},\mathcal{R},\gamma\right) \tag{27}$$

where S is the state space, A is the action space, P is the transition probability, R is the reward function, and γ is the discount factor. The objective of the agent is to learn a policy that maximizes the accumulated discounted reward:

$$G_k=\sum_{i=0}^{\infty}\gamma^{i}r_{k+i} \tag{28}$$

where G_k is the return from time step k, r_{k+i} is the future reward, and γ determines the importance of future rewards.

Table 3 summarizes the RL components used in the proposed EMS. In this formulation, the learning agent represents the EMS controller, while the environment represents the dynamic response of the PV arrays, wind turbine, BESS, DC bus, grid switch, and cold-ironing load.

Table 3. Reinforcement-learning components used in the proposed energy management system (EMS)

RL component	**Definition in the proposed system**
Agent	Learning-based EMS controller
Environment	PV arrays, wind turbine, BESS, DC bus, grid switch, and cold-ironing load
State	Measured operating condition of the system
Action	Control commands for BESS operation and PV control mode
Reward	Performance measure based on voltage regulation, SOC limits, grid use, and control smoothness

Abbreviations: BESS: Battery energy storage system; DC: Direct current; PV: Photovoltaic; RL: Reinforcement learning; SOC: State of charge.

At each time step, the agent observes the current state, selects an action, receives a reward, and observes the next system state. This interaction can be expressed as:

$$s_k\xrightarrow{a_k}r_k,s_{k+1} \tag{29}$$

where s_k is the current state, a_k is the selected action, r_k is the reward, and s_{k+1} is the next state.

3.4. Deep deterministic policy gradient-based energy management system design

Deep deterministic policy gradient is selected because the proposed EMS requires continuous control actions rather than only discrete switching decisions. The controller must generate a continuous battery power command and supervise the operating condition of the RES. For the PV arrays, the EMS determines whether the PV subsystem should remain in MPPT operation or shift to PI-based power-limiting mode during excess-generation conditions. The wind subsystem is supervised through its available MPPT power contribution and coordinated with PV generation and BESS operation to maintain the DC-bus voltage and ensure reliable cold-ironing supply.

Deep deterministic policy gradient is suitable for continuous-control problems because it combines a deterministic actor policy with a critic network that evaluates the quality of the selected action.[43,44] The deterministic actor policy is expressed as:

$$a_k = \mu\left(s_k \mid \theta^{\mu}\right) \tag{30}$$

where a_k is the selected action, s_k is the observed state, μ is the actor policy, and ϑ^{μ} represents the actor network parameters. The critic network estimates the action-value function:

$$Q\left(s_k, a_k \mid \theta^{Q}\right) \tag{31}$$

where Q is the expected return of applying action a_k in state s_k, and ϑ^{Q} represents the critic network parameters.

The DDPG action vector contains two control components:

$$a_k = \left[a_{\mathrm{bat}}(k) a_{\mathrm{PV}}(k)\right] \tag{32}$$

where a_{bat} is the battery control action, and a_{PV} is the PV control action. The battery action controls BESS charging or discharging, while the PV action supervises the PV operating mode between MPPT and power-limiting control. Flexible PV power control is useful in DC microgrids when available PV generation exceeds load demand or storage capability.[45]

The battery action is bounded within the continuous range:

$$-1 \le a_{\mathrm{bat}}(k) \le 1 \tag{33}$$

and mapped to the battery power reference as:

$$P^{*}_{\mathrm{bat}}(k) = a_{\mathrm{bat}}(k) P_{\mathrm{bat,max}} \tag{34}$$

where $P_{bat,max}$ is the maximum allowable battery power. Positive values represent battery discharge, while negative values represent battery charging. The PV action is mapped to the PV power reference as:

$$P^{*}_{\mathrm{PV}}(k) = \alpha_{\mathrm{PV}}(k) P_{\mathrm{PV,avail}}(k) \tag{35}$$

where $P_{\mathrm{PV,avail}}$ is the available PV power, and a_{PV} is the PV power-limiting factor. When a_{PV} is close to unity, the PV subsystem operates near MPPT mode. When a_{PV} is reduced, the EMS shifts the PV subsystem toward power-limited operation to prevent overvoltage or battery overcharging during excess generation conditions.

3.5. State-space representation

The DDPG state vector is designed to provide the agent with the main variables required for energy-management decisions. The observation vector includes the normalized DC-bus voltage error, battery SOC, load demand, PV power, wind power, time-cycle information, and emergency grid usage. The state vector is defined as:

$$s_k = \begin{bmatrix} e_{v,n}(k) \\ SOC(k) \\ P_{load,n}(k) \\ P_{PV,n}(k) \\ P_{WT,n}(k) \\ \sin\left(\dfrac{2\pi h_k}{24}\right) \\ \cos\left(\dfrac{2\pi h_k}{24}\right) \\ u_{grid}(k) \end{bmatrix}^{T} \tag{36}$$

where $e_{v,n}$ is the normalized voltage error, SOC is the battery state of charge, $P_{\mathrm{load},n}$, $P_{\mathrm{PV},n}$, and $P_{\mathrm{WT},n}$ are normalized load, PV, and wind powers, respectively, h_k is the hour index in the daily profile, and u_{grid} is the emergency grid-switch indicator.

The normalized voltage error is calculated as:

$$e_{v,n}(k) = \frac{V_{\mathrm{dc}}(k) - V_{\mathrm{dc,ref}}}{V_{\mathrm{dc,ref}}} \tag{37}$$

Power variables are normalized using the base power:

$$P_{x,n}(k) = \frac{P_x(k)}{P_{\mathrm{base}}} \tag{38}$$

where P_x may represent load power, PV power, wind power, or grid power. The sine and cosine time-cycle terms are included to avoid discontinuity between hour 24 and hour 0 and to help the agent recognize daily renewable-generation patterns.

3.6. Environment dynamics and reward function

The DDPG training environment represents the main dynamic behavior of the proposed cold-ironing DC microgrid. After applying an action, the environment updates renewable power, battery power, SOC, DC-bus voltage, PV operating mode, grid-switch status, reward value, and the next observation. The environment transition is written as:

$$s_{k+1} = f\left(s_k, a_k, w_k\right) \tag{39}$$

where w_k represents external inputs such as irradiance, temperature, wind speed, and load demand.

For efficient training, the DC-bus voltage response is represented using a simplified voltage-sensitivity model:

$$V_{\mathrm{dc}}\left(k+1\right) = V_{\mathrm{dc}}\left(k\right) + K_v \begin{bmatrix} P_{\mathrm{RES}}\left(k\right) + P_{\mathrm{bat}}\left(k\right) \\ +P_{\mathrm{grid}}\left(k\right) - P_{\mathrm{load}}\left(k\right) \end{bmatrix} \tag{40}$$

where K_v is the voltage-sensitivity coefficient. This simplified model is used only during DDPG training to reduce computational burden. The final control policy is then evaluated using the complete MATLAB/Simulink model.

The battery SOC is updated according to the energy balance:

$$SOC\left(k+1\right) = SOC\left(k\right) - \frac{P_{\mathrm{bat}}\left(k\right)\Delta t}{E_{\mathrm{bat}}} \tag{41}$$

where Δt is the simulation time step, and E_{bat} is the rated battery energy capacity. Since positive P_{bat} represents discharge, the SOC decreases when $P_{\mathrm{bat}} > 0$ and increases when $P_{\mathrm{bat}} < 0$.

Reward design is important in RL-based microgrid energy management because it directly shapes the learned dispatch policy.[46] In this study, the reward function was designed to encourage DC-bus voltage stability, safe battery SOC operation, backup-grid activation only during standalone RES-system failure, smooth battery operation, and avoidance of unnecessary PV curtailment. The reward is formulated as the negative sum of weighted operating penalties:

$$r_k = -\begin{pmatrix} w_v C_v\left(k\right) + w_g C_g\left(k\right) \\ +w_{soc} C_{soc}\left(k\right) + w_b C_b\left(k\right) + w_{pv} C_{pv}\left(k\right) \end{pmatrix} \tag{42}$$

where C_v is the voltage-deviation cost, C_g is the backup-grid activation cost, C_{SOC} is the SOC violation penalty, C_b is the battery-usage cost, and C_{pv} is the PV power-limiting cost. The voltage-deviation cost is defined as:

$$C_v\left(k\right) = \left(\frac{V_{\mathrm{dc}}\left(k\right) - V_{\mathrm{dc,ref}}}{V_{\mathrm{dc,ref}}}\right)^2 \tag{43}$$

The SOC violation penalty is:

$$C_{soc}\left(k\right) = \max\begin{pmatrix} 0, SOC_{\min} - SOC\left(k\right))^2 \\ +\max\left(0, SOC\left(k\right) - SOC_{\max})^2\right) \end{pmatrix} \tag{44}$$

The battery-usage cost is:

$$C_b\left(k\right) = \left(\frac{P_{\mathrm{bat}}\left(k\right)}{P_{\mathrm{bat,max}}}\right)^2 \tag{45}$$

The PV power-limiting cost is:

$$C_{pv}\left(k\right) = \left(1 - \alpha_{\mathrm{PV}}\left(k\right)\right)^2 \tag{46}$$

This term discourages unnecessary PV curtailment during normal operation, while the voltage and SOC penalties encourage PV limitation when excess generation may cause DC-bus overvoltage or battery overcharging. The reward-function components are summarized in **Table 4**.

3.7. Deep deterministic policy gradient training and implementation workflow

The DDPG agent is trained using an actor network, critic network, replay buffer, target networks, and exploration noise. The actor receives the observation vector and generates two continuous control actions. The critic receives both the state and the action and estimates the expected return of the selected EMS decision. **Figure 13** shows the DDPG-based EMS workflow used for training and control implementation.

The critic target value is calculated as:

$$y_k = r_k + \gamma Q'\left(s_{k+1}, \mu'(s_{k+1}\middle|\theta^{\mu'}) \middle|\theta^{Q'}\right) \tag{47}$$

where Q’ and μ’ are the target critic and target actor networks, respectively. The critic network is trained by minimizing the mean-squared error loss:

$$L\left(\theta^{Q}\right)=\frac{1}{N}\sum_{i=1}^{N}\left(y_i-Q\left(s_i,a_i\mid\theta^{Q}\right)\right)^2 \quad (48)$$

Table 4. Reward-function components used in the DDPG-based EMS

Reward component	**Purpose**
Voltage-deviation cost	Keeps V_{dc} close to $V_{\mathrm{dc,ref}}$
Backup-grid activation cost	Limits grid activation to failure conditions of the standalone RES system
SOC violation penalty	Prevents battery overcharge and deep discharge
Battery-usage cost	Reduces aggressive battery cycling
PV power-limiting cost	Avoids unnecessary PV curtailment

Abbreviations: DDPG: Deep deterministic policy gradient; EMS: Energy management system; PV: Photovoltaic; RES: Renewable energy sources; SOC: State of charge.

where N is the mini-batch size. The target networks are updated using soft updates:

$$\theta'\leftarrow\tau\theta+\left(1-\tau\right)\theta' \quad (49)$$

where τ is the target smoothing factor. Soft updating improves training stability by preventing sudden changes in target-network parameters.

Several implementation refinements are introduced to stabilize training and ensure physically meaningful control commands. These include observation normalization, bounded actor outputs, physical command saturation, SOC protection, action smoothing, reward weighting, PV MPPT/PI supervision, and simplified environment dynamics. These refinements are necessary because DDPG uses neural networks for both the actor and critic approximation, and poor input scaling or poorly bounded actions can lead to unstable learning behavior.[44] The main training refinements are summarized in **Table 5**.

After training, the learned DDPG policy is evaluated under the same operating scenarios used for the conventional EMS. This enables a fair comparison between the deterministic rule-based controller and the adaptive learning-based

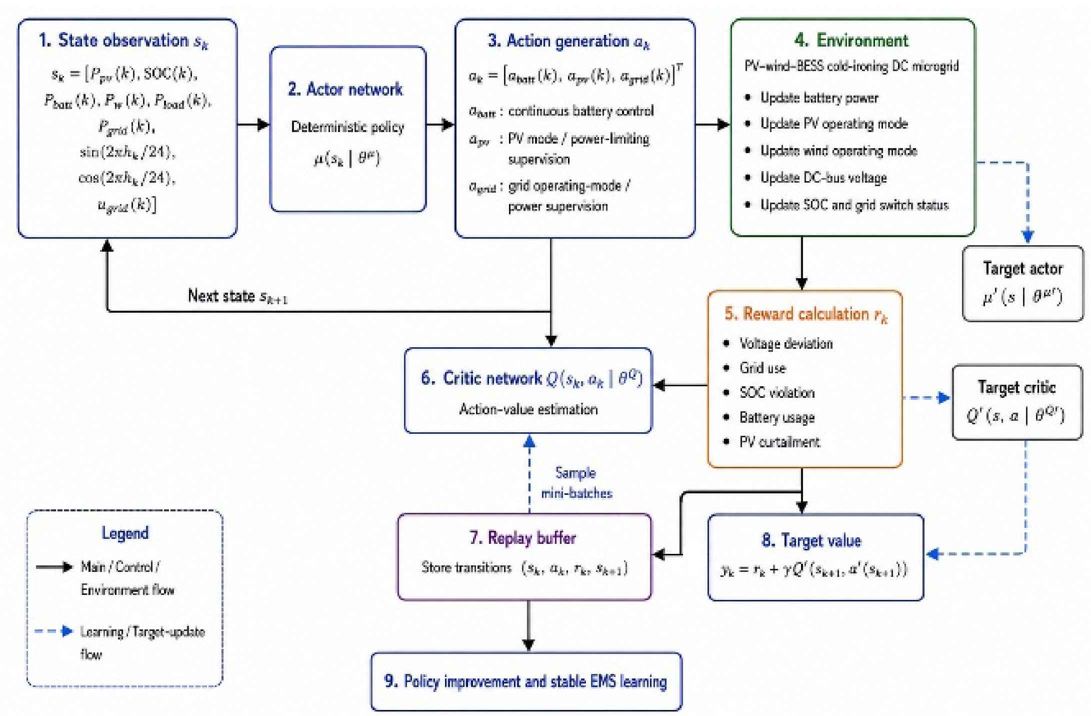

Figure 13. DDPG-based EMS workflow showing state observation, actor action generation, environment update, reward calculation, critic evaluation, replay-buffer learning, and target-network update
Abbreviations: BESS: Battery energy storage system; DC: Direct current; DDPG: Deep deterministic policy gradient; EMS: Energy management system; PV: Photovoltaic; SOC: State of charge.

EMS under equivalent renewable-generation, load-demand, SOC, and DC-bus conditions.

Table 5. Training stabilization refinements used in the DDPG-based EMS

Refinement	Purpose
Observation normalization	Reduces numerical imbalance between state variables
Bounded action outputs	Keeps actor commands within valid operating ranges
Physical saturation	Prevents battery and PV commands from exceeding limits
SOC protection	Blocks unsafe charging or discharging
Reward weighting	Prioritizes voltage stability, SOC safety, and reduced grid use
Action smoothing	Reduces sudden battery command variations
PV MPPT/PI supervision	Allows switching between MPPT and PV power-limiting operation
Simplified training environment	Reduces computational burden during DDPG training

Abbreviations: DDPG: Deep deterministic policy gradient; EMS: Energy management system; MPPT: Maximum power point tracking; PI: Proportional integral; PV: Photovoltaic; SOC: State of charge.

4. Simulation results and comparative evaluation

4.1. Simulation setup and performance indicators

The proposed PV–wind–BESS cold-ironing DC microgrid was developed and evaluated in MATLAB R2024a/Simulink (MathWorks, United States of America). The complete model includes a 2 MW PV subsystem composed of two independently controlled PV arrays, a 1 MW PMSG wind turbine, a 1 MWh BESS, a regulated 1,000 V DC bus, a shore-side cold-ironing conversion unit, and a backup grid interface activated only in case of failure of the standalone RES system. The cold-ironing load is represented as a constant 2 MW active-power demand to reflect a fixed berth-supply requirement. The simulation study evaluated the ability of the EMS to maintain DC-bus voltage stability, coordinate renewable generation, manage BESS charging and discharging, and activate backup grid support only if the standalone RES system cannot maintain the required load supply.

The main performance indicators used to evaluate system operation were DC-bus voltage deviation, battery SOC variation, RES response, BESS operating mode, and backup-grid activation requirement in case of standalone RES-system failure. The DC-bus voltage deviation is calculated as:

$$\Delta V_{\mathrm{dc}}(k) = V_{\mathrm{dc}}(k) - V_{\mathrm{dc,ref}} \tag{50}$$

where $V_{\mathrm{dc,ref}}$ is the 1,000 V reference DC-bus voltage. The percentage voltage deviation is expressed as:

$$\Delta V_{\mathrm{dc,\%}}(k) = \frac{V_{\mathrm{dc}}(k) - V_{\mathrm{dc,ref}}}{V_{\mathrm{dc,ref}}} \times 100 \tag{51}$$

The net renewable power balance is evaluated using:

$$\Delta P_{\mathrm{RES}}(k) = P_{\mathrm{RES}}(k) - P_{\mathrm{load}}(k) \tag{52}$$

where positive ΔP_{RES} indicates surplus renewable generation and negative ΔP_{RES} indicates renewable power shortage. These indicators were used to interpret the conventional EMS results, the DDPG-based EMS results, and the comparative assessment between the two control strategies.

4.2. Conventional energy management system performance under representative operating cases

The conventional rule-based EMS was first evaluated under different renewable-generation conditions. The purpose of this stage was to verify the baseline capability of the proposed HRES to supply the cold-ironing load, maintain the DC-bus voltage close to 1,000 V, and protect the battery under normal, shortage, and excess-generation conditions. The tested scenarios are summarized in **Figure 14**.

Under the nominal operating case, the two PV arrays operated under MPPT control and generated approximately 2 MW, while the wind turbine contributed approximately 1 MW. Since the cold-ironing load was fixed at 2 MW, the total renewable generation exceeded the load requirement. As shown in **Figure 15A**, the DC-bus voltage remained regulated close to

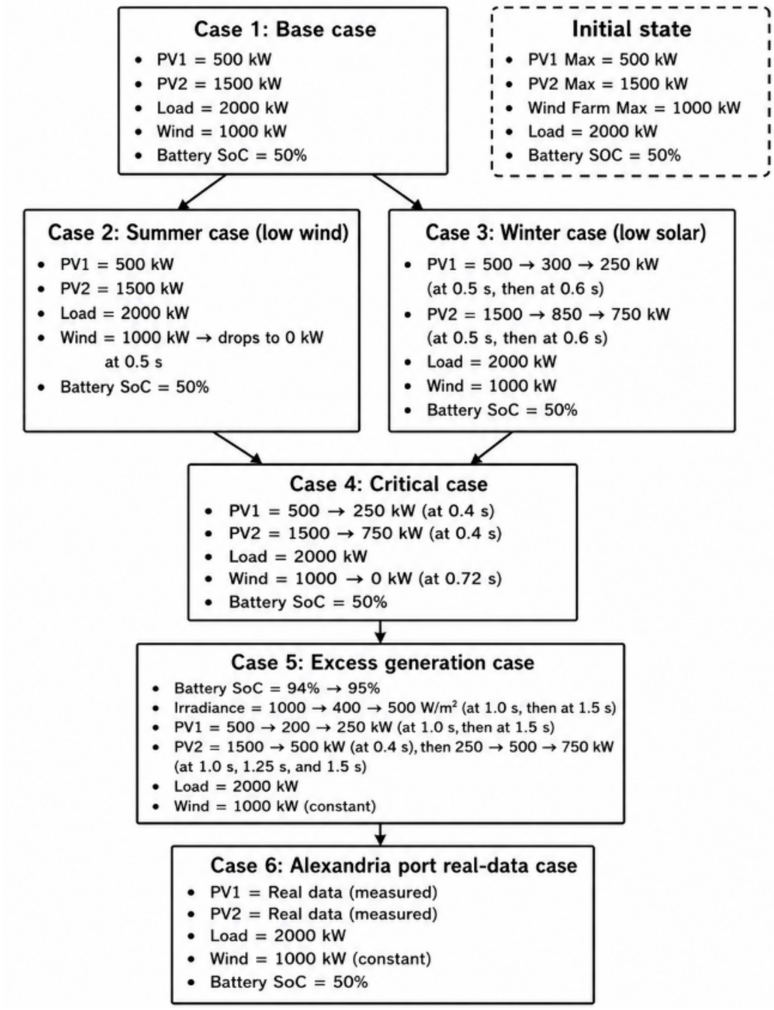

Figure 14. Simulation scenarios used to evaluate the conventional EMS under normal operation, renewable-power shortage, excess-generation, and real-data operating conditions

Abbreviations: EMS: Energy management system; PV: Photovoltaic; SOC: State of charge.

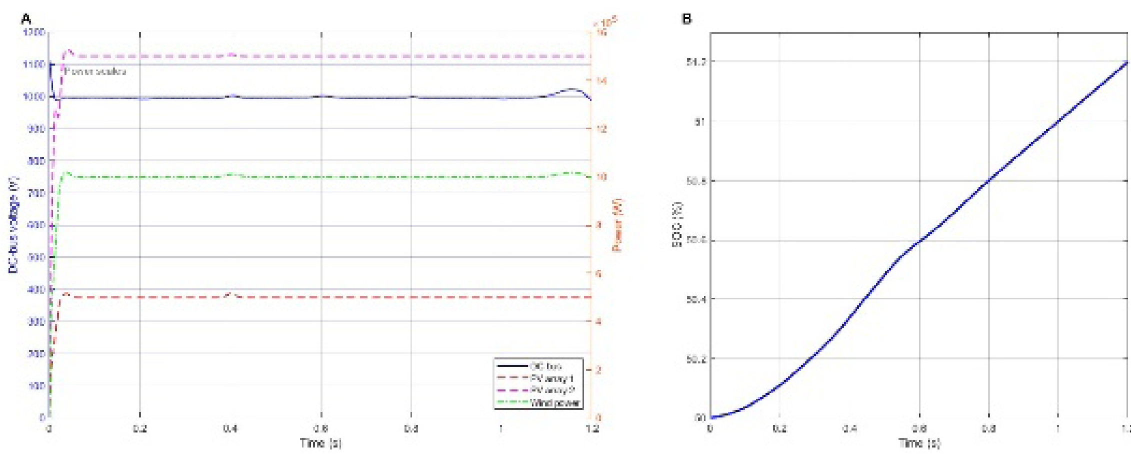

Figure 15. Conventional energy management system response under nominal operation. (A) Direct current (DC)-bus voltage and renewable power generation. (B) Battery state-of-charge (SOC) variation during surplus renewable generation.

1,000 V despite the presence of surplus renewable power. The excess generation was directed to the BESS, and the battery SOC increased gradually, as shown in **Figure 15B**. This confirms that the conventional EMS can maintain stable standalone RES-based operation when renewable generation is sufficient and storage capacity is available.

The second representative case evaluated wind power loss under PV-dominant operation. In this case, the wind turbine output drastically dropped from approximately 1 MW to zero, while the two PV arrays continued supplying the cold-ironing load. **Figure 16A** shows that the DC-bus voltage experienced only a small transient deviation before returning close to the 1,000 V reference. The battery SOC response in **Figure 16B** shows that the battery transitioned from charging operation to a near-floating state because PV generation remained sufficient to supply the fixed cold-ironing load after the wind drop. Therefore, the backup grid was not activated because the standalone RES/BESS system maintained the load supply.

A further shortage case was examined by reducing solar irradiance while keeping the wind turbine available. As shown in **Figure 17A**, the PV power decreased after the irradiance drop, but the wind turbine continued supporting the DC bus. The EMS kept the PV arrays in MPPT mode under reduced irradiance conditions, while the BESS provided light support or continued limited charging depending on the available power balance. **Figure 17B** shows that the SOC remained within the safe operating range. The DC-bus voltage remained close to the reference value, confirming that the combined wind and BESS response can compensate for the PV reduction without activating the backup grid.

The most severe conventional EMS case considered sequential PV and wind power loss. In this case, PV output decreased first, followed by a reduction in wind power. As shown in **Figure 18A**, the DC-bus voltage remained regulated at around 1,000 V with limited transient deviations during renewable power disturbances. The SOC response in **Figure 18B** confirms that the BESS changed its operating mode according to the power balance requirement. Initially, the battery can absorb surplus power; after the renewable deficit appears, it discharges to support the DC bus and maintain load supply. This case confirms that the conventional EMS can preserve system stability under combined renewable disturbances when the battery has sufficient SOC.

An excess-generation case was also evaluated to test the ability of the conventional EMS to protect the BESS when the battery approaches the upper SOC limit. In this case, renewable generation initially exceeded the 2 MW cold-ironing load, while the battery SOC was high. As shown in **Figure 19**, the EMS activated PV power-limiting control when further battery charging was not desirable. Instead of allowing uncontrolled DC-bus voltage rise or battery overcharging, the controller shifted the PV subsystem from MPPT operation to PI-based

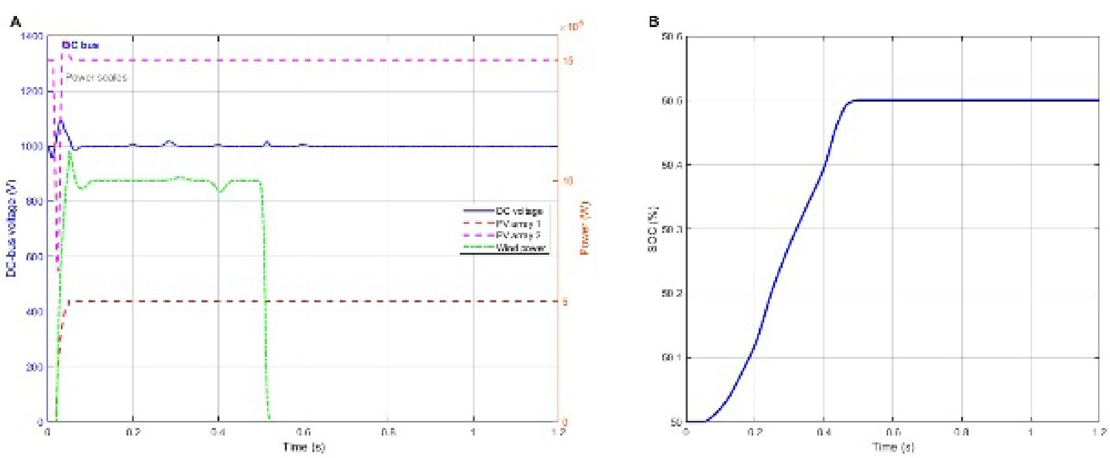

Figure 16. Conventional energy management system response during wind power loss. (A) Direct current (DC)-bus voltage and renewable generation response. (B) Battery state-of-charge (SOC) response during transition from surplus generation to power balance.

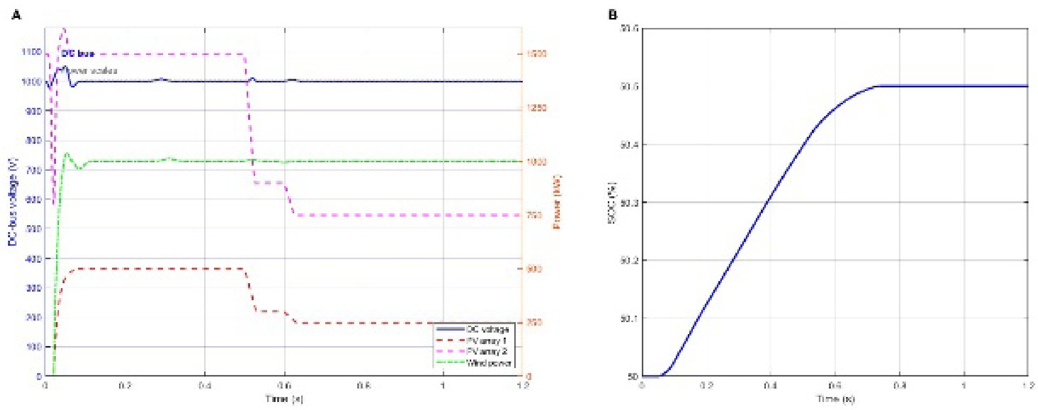

Figure 17. Conventional energy management system response under photovoltaic (PV) power reduction. (A) Direct current (DC)-bus voltage and renewable power output during an irradiance drop. (B) Battery state-of-charge (SOC) response during reduced PV generation.

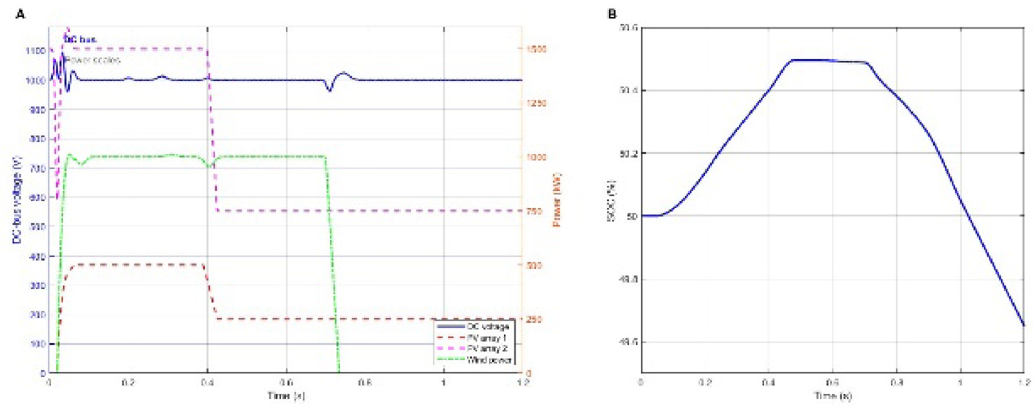

Figure 18. Conventional energy management system response during sequential photovoltaic (PV) and wind power loss. (A) Direct current (DC)-bus voltage and renewable power output. (B) Battery state-of-charge (SOC) response during staggered renewable-power reduction.

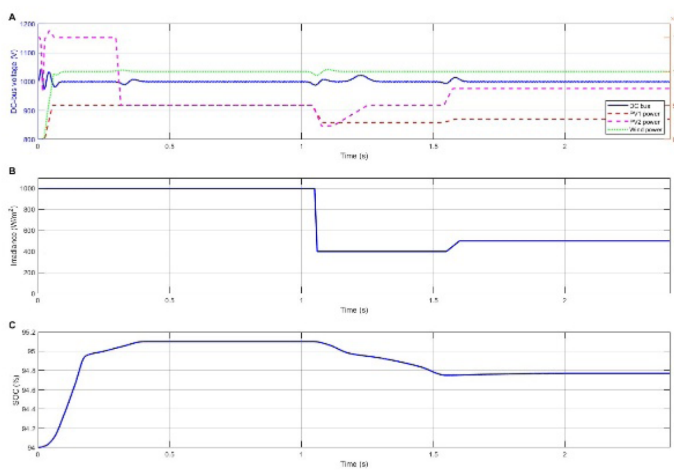

Figure 19. Conventional energy management system response under excess renewable generation with photovoltaic (PV) power-limiting control and battery state-of-charge (SOC) protection. (A) DC-bus voltage and renewable power response. (B) Solar irradiance profile. (C) Battery state-of-charge (SOC) response.

power-limiting mode. The DC-bus voltage remained close to 1,000 V, and the battery SOC was prevented from exceeding the allowable operating range.

Overall, the conventional EMS served as a benchmark for comparing the performance of the proposed adaptive DDPG-based EMS. The rule-based controller supplied the load, maintained the DC-bus voltage near its reference value, charged the battery during surplus generation, discharged the battery during renewable shortage, and activated PV limitation when the SOC approached its upper limit. However, its response remained dependent on fixed thresholds and predefined operating modes, prompting the adoption of an adaptive DDPG-based EMS.

4.3. Alexandria Port real-data validation case

To examine the practical applicability of the proposed system, a real-data case study was conducted using meteorological data from Alexandria Port. Solar irradiance and wind-related inputs were obtained from National Aeronautics and Space Administration (NASA) Prediction of Worldwide Energy Resource (POWER) meteorological data for the Alexandria Port and entered into the simulation environment through an Excel-based input profile.[47] The identified onshore PV installation areas considered in the port case study are shown in **Figure 20**. These areas include a larger zone assigned to the 1.5 MW PV array and a second zone assigned to the 0.5 MW PV array.

The dynamic response from the Alexandria Port case is shown in **Figure 21**. **Figure 21A** shows that the PV power varied with the solar input profile, while the wind turbine provided continuous renewable support to the DC bus according to the available wind resource. PV Farm 1's power increased gradually and reached approximately 500 kW, while that of PV Farm 2 reached 1.5–1.6 MW during peak generation. After the solar peak, both PV outputs decreased as irradiance decreased. Despite these renewable variations, the DC-bus voltage remained close to 1,000 V with only minor transient deviations. **Figure 21B** shows that the battery SOC started at approximately 50%, decreased slightly during the early period when PV generation was low, recovered during periods of higher renewable generation, and decreased again toward the end as PV power decreased.

The Alexandria Port case confirms that the proposed HRES can maintain stable cold-ironing operation under realistic environmental conditions. Although PV generation varied significantly with the irradiance profile, the wind turbine and BESS maintained the DC bus voltage within the required power balance. The voltage response remained close to the 1,000 V reference, validating the robustness of the proposed system for renewable-powered cold ironing in Mediterranean and North-African coastal ports.

4.4. Deep deterministic policy gradient-based energy management system performance

After verifying the system using the conventional EMS, the DDPG-based EMS was evaluated under three representative cases: base operation, critical renewable shortage, and excess renewable generation. These cases were selected because they directly test the key control objectives of the RL-based EMS: maintaining DC-bus voltage stability, coordinating BESS response, supervising PV and wind operation, and activating backup grid support only in the event of a standalone RES-system failure. The DDPG simulation scenarios are summarized in **Figure 22**.

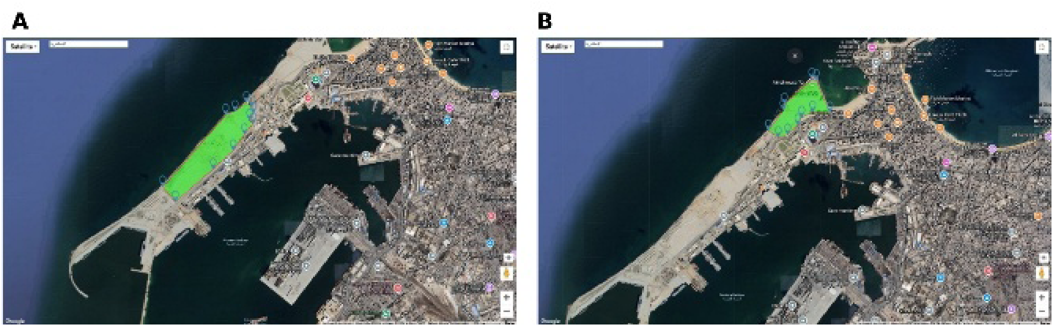

Figure 20. Identified onshore photovoltaic (PV) installation areas at Alexandria Port. (A) PV Area 1 assigned to the 1.5 MW PV array. (B) PV Area 2 assigned to the 0.5 MW PV array.

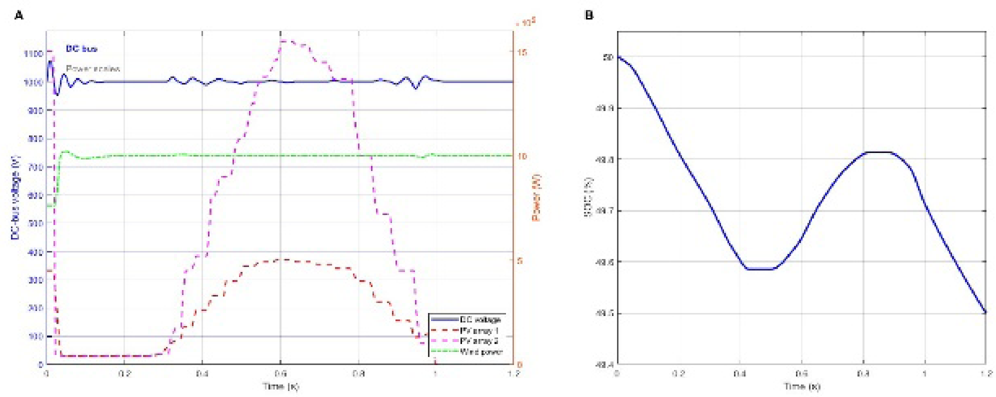

Figure 21. Alexandria Port real-data case: (a) DC-bus voltage and renewable power response and (b) battery SOC response under realistic meteorological input conditions.

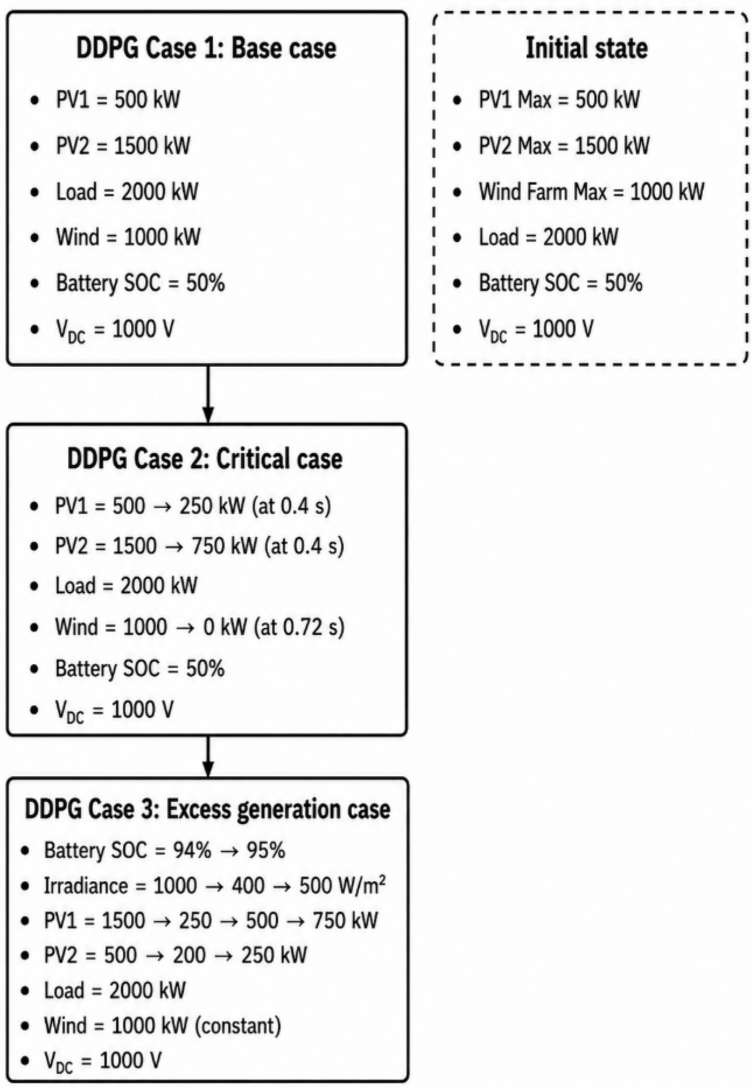

Figure 22. Deep deterministic policy gradient simulation scenarios used to evaluate base operation, critical renewable shortage, and excess renewable generation
Abbreviations: PV: Photovoltaic; SOC: State of charge.

4.4.1. Deep deterministic policy gradient base case

The DDPG base case represented normal operation with constant solar irradiance of 1,000 W/m², wind speed of 12 m/s, and an initial battery SOC of 50%. Under this case, PV Farm 1 generated approximately 1.5 MW, PV Farm 2 generated approximately 0.5 MW, and the wind turbine generated approximately 1.0 MW. Therefore, the total renewable generation reached approximately 3 MW, while the cold-ironing load remained at 2 MW.

As shown in **Figure 23A**, the DDPG controller maintained the DC-bus voltage near 1,000 V while the PV arrays and wind turbines supplied the load. Since total renewable generation exceeded the load demand, the surplus renewable power was directed to the BESS. **Figure 23B** shows that the battery SOC increased gradually from 50% to 51.2%, confirming that the DDPG-based EMS charges the battery smoothly using the excess renewable energy. The backup grid was not activated because the standalone RES/BESS system maintained the load supply.

4.4.2. Deep deterministic policy gradient critical renewable-shortage case

The DDPG critical case evaluated the response of the proposed EMS to sequential renewable-power disturbances. Initially, PV Farm 1 generated 1.5 MW, PV Farm 2 generated 0.5 MW, and the wind turbine generated 1 MW. At 0.4 s, the PV power dropped as PV Farm 1 decreased from 1.5 MW to 0.75 MW and PV Farm 2 decreased from 0.5 MW to 0.25 MW. At 0.75 s, the wind turbine output dropped from 1 MW to 0 MW, leading to a severe renewable-generation shortage.

As shown in **Figure 24A**, the DDPG-based EMS maintained the DC-bus voltage around 1,000 V throughout the disturbances. During the initial surplus period, the battery was charged, and the SOC increased from 50% to 50.5%, as shown in **Figure 24B**. After the PV reduction, the remaining PV and wind power were close to the load requirement, and the battery entered a near-floating condition. When the wind turbine output dropped to zero, the battery transitioned to discharge mode to compensate for the renewable-generation deficit. The SOC decreased from 50.5% to 50.05%, confirming that the battery supplies the required support without violating its operating limits.

The DDPG critical case demonstrates that the trained controller coordinated battery operation smoothly in response to sudden renewable disturbances. The DC-bus voltage remained close to its reference value, and the backup grid was not activated because the standalone RES/BESS system maintained the load supply. These results indicate that the DDPG-based EMS can effectively utilize available BESS capacity to maintain stable cold-ironing operation during short-term renewable energy shortages.

4.4.3. Deep deterministic policy gradient excess-generation case

The DDPG excess-generation case evaluated the ability of the controller to manage surplus

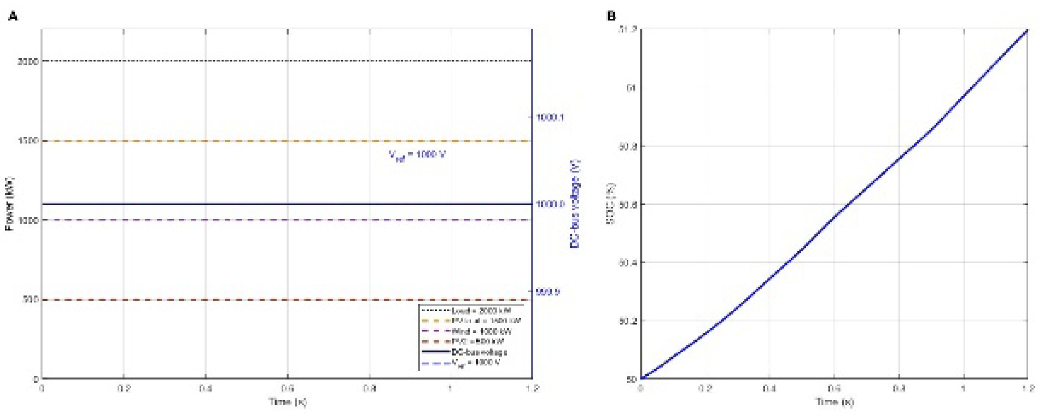

Figure 23. Deep deterministic policy gradient base case response. (A) Direct current (DC)-bus voltage and renewable power response under normal operation. (B) Battery state-of-charge (SOC) response during smooth surplus-power charging.

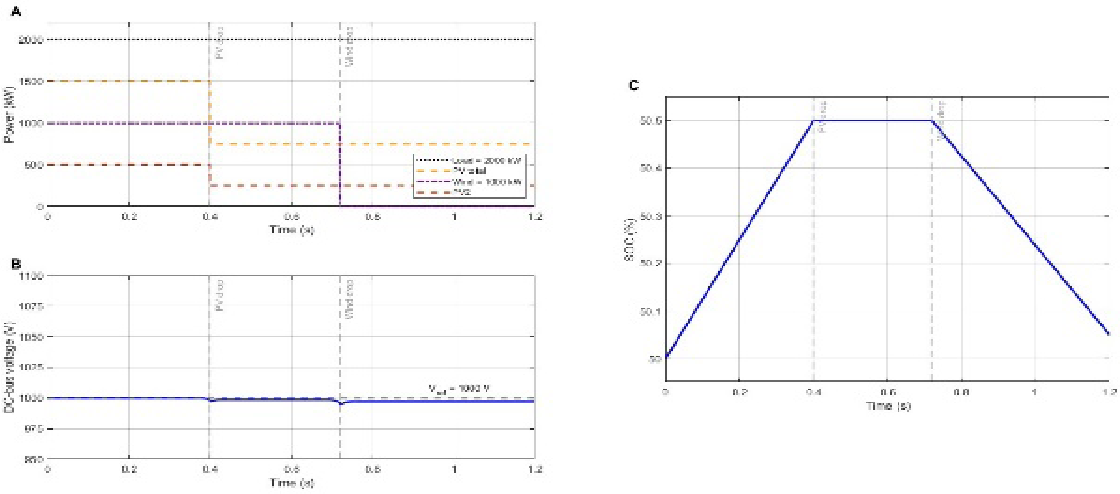

Figure 24. Deep deterministic policy gradient critical case response. Direct current (DC)-bus (A) power and (B) voltage response under photovoltaic (PV) and wind power reduction. (C) Battery state-of-charge (SOC) response during charging, floating, and discharging operation.

renewable power when the battery is close to its upper SOC limit. The initial battery SOC was 94%, and the system began with PV generation of approximately 2 MW and wind generation of approximately 1 MW, while the load remained fixed at 2 MW. Therefore, the total renewable generation initially exceeded the load demand by approximately 1 MW.

As shown in **Figure 25A**, the DDPG-based EMS initially directed the surplus renewable energy to the battery. Consequently, the battery SOC increased from 94% to 95.1%, as shown in **Figure 25B**. Once the battery approached its upper operating limit, the DDPG controller activated overcharge protection by switching the PV subsystem from MPPT operation to PI-based power-limiting operation. This reduced PV output and prevented continued battery overcharging. In the same case, irradiance decreased from 1,000 W/m^2 to 400 W/m^2, then recovered to 500 W/m^2. The controller continuously supervised the RES response, coordinated PV limitation, maintained wind contribution, and sustained the DC-bus voltage around 1,000 V with only minor transient deviations.

The excess-generation case confirms that the DDPG-based EMS can handle high-SOC operation without activating the backup grid. By coordinating PV power limitation, wind contribution, and battery protection, the DDPG controller maintains stable cold-ironing operation under surplus renewable generation.

4.5. Comparative evaluation between conventional and deep deterministic policy gradient-based energy management system

The comparative assessment focuses on the operating cases tested using both control strategies: base operation, critical renewable shortage, and excess renewable generation. The conventional EMS depends on fixed rules and threshold-based transitions, while the DDPG-based EMS uses a learned control policy to determine the appropriate control action according to the system state.

Both EMS strategies maintained the DC-bus voltage close to the reference value of 1,000 V and supplied the cold-ironing load under the tested conditions (**Table 6**). However, the DDPG-based EMS provided a smoother and more adaptive response. In the base case, the DDPG controller maintained a very smooth voltage response while charging the battery steadily using surplus renewable power. In the critical case, the DDPG controller reduced the impact of PV and wind power drops by coordinating the battery discharge response more effectively. In the excess-generation case, it managed the high-SOC condition by reducing PV output and limiting surplus power generation, thereby preventing battery overcharging and supporting voltage stability. The backup-grid activation requirement was therefore limited to failure conditions of the standalone RES system, and no backup-grid

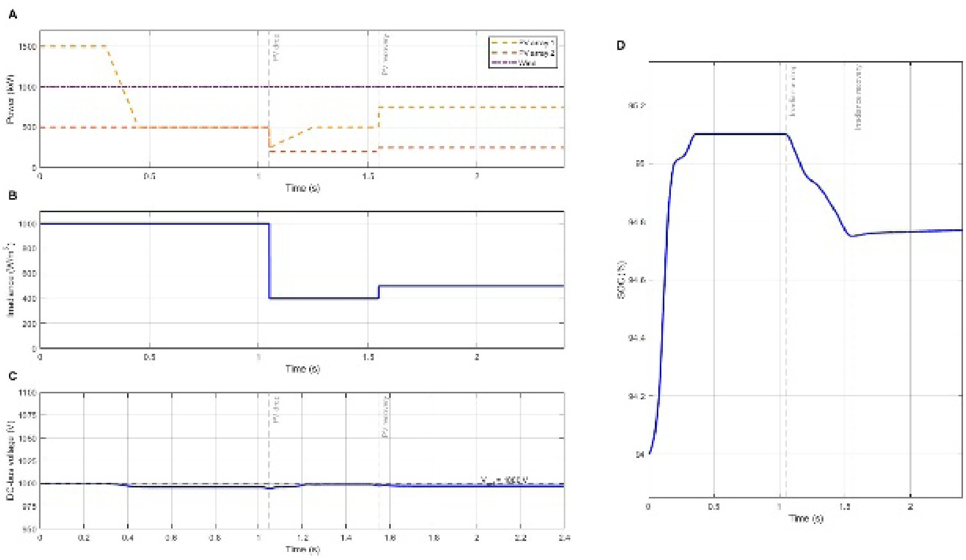

Figure 25. Deep deterministic policy gradient excess-generation case response. (A) Renewable power, (B) solar irradiance profile, and (C) direct current (DC)-bus voltage response during surplus generation and photovoltaic (PV) power limitation. (D) Battery state-of-charge (SOC) response near the upper operating limit.

Table 6. Comparative performance between the conventional and deep deterministic policy gradient (DDPG)-based energy management system (EMS)

Performance aspect	**Conventional EMS**	**DDPG-based EMS**
Control strategy	Rule-based logic using predefined thresholds	Learned control policy based on system states
Base case operation	Stable DC-bus voltage with minor transients	Very smooth voltage response close to 1,000 V
Critical case response	Battery discharges after renewable power shortage	Battery response is smoother, and voltage deviation is reduced
Excess power management	EMS limits surplus power by changing PV control from MPPT to PI-based control	DDPG coordinates PV power reduction and battery SOC protection more smoothly
DC-bus voltage stability	Maintains close to 1,000 V in all cases	Maintains closer to the reference value with smaller fluctuations
Battery SOC behavior	Charging and discharging follow rule-based transitions	SOC changes more smoothly according to learned control action
RES coordination	PV, wind, and battery are coordinated using fixed logic	PV, wind, and battery are coordinated dynamically
Backup-grid activation requirement	Activated only in case of standalone RES-system failure	Activated only in case of standalone RES-system failure; not activated in the tested representative cases
Response to disturbances	Stable but more dependent on switching thresholds	Faster and smoother response to sudden changes

Abbreviations: DC: Direct current; MPPT: Maximum power point tracking; PI: Proportional integral; PV: Photovoltaic; RES: Renewable energy sources; SOC: State of charge.

activation was observed in the representative DDPG cases because the standalone RES/BESS system maintained the cold-ironing load supply.

The results indicate that the conventional EMS is sufficient for maintaining stable operation when the system conditions match predefined control rules. Meanwhile, the DDPG-based EMS improves dynamic behavior by adjusting the battery action and RES supervision according to the observed system state. This leads to smoother SOC variation in the battery, reduced voltage fluctuations, and more flexible coordination among PV generation, wind generation, and BESS operation. Therefore, the DDPG-based EMS provides an enhanced control approach for renewable-powered cold-ironing DC microgrids operating under variable-generation conditions, while limiting backup grid support to failure conditions of the standalone RES system.

5. Discussion

The simulation results confirm that the proposed PV–wind–BESS cold-ironing DC microgrid can maintain stable operation under different renewable-generation conditions. Across the tested cases, the 1,000 V DC bus remained close to its reference value, while the BESS absorbed surplus renewable power during high-generation periods and discharged during renewable-power shortages. This behavior confirms the importance of storage in renewable-powered shore-side supply systems, where the mismatch between intermittent generation and fixed ship-load demand must be managed continuously. Previous studies have also emphasized that battery storage is essential for improving reliability and renewable-energy integration in high-power port and microgrid applications.[7,8]

The conventional EMS provides a practical baseline because it coordinates the PV arrays, wind turbine, BESS, and backup grid interface using predefined operating modes. Its rule-based structure is simple to implement and can maintain stable operation when the system operates within expected conditions. During surplus renewable generation, the conventional EMS directs excess power to the battery. During renewable-power shortage, it allows the battery to discharge and support the DC bus. When the battery approaches its upper SOC limit, the EMS switches the PV subsystem from MPPT operation to PI-based power-limiting control. This confirms that a deterministic EMS can provide acceptable control performance for standalone renewable-powered cold ironing when the operating conditions are clearly defined.

The main limitation of the conventional EMS is its dependence on fixed thresholds and predefined transitions. In a renewable-powered cold-ironing system, PV power, wind power, battery SOC, and DC-bus voltage may change simultaneously. A rule-based controller can respond to these changes, but its response is limited by the logic designed before simulation. This issue becomes more important in critical and excess-generation cases, where the controller must balance multiple objectives simultaneously, including voltage regulation, SOC protection, RES coordination, and continuous load supply. Similar limitations have been reported in microgrid EMS studies, where conventional strategies can become less flexible under uncertain renewable generation and dynamic operating conditions.[10,12]

The DDPG-based EMS addresses this limitation by generating continuous control actions according to the observed system state. Unlike simple switching logic, the DDPG agent uses voltage error, SOC, load demand, PV power, wind power, time-cycle information, and backup-grid status to determine the appropriate control response. This is suitable for the proposed system because battery charging and discharging are not only ON/OFF decisions; they require continuous power control. DRL is effective for microgrid control problems involving nonlinear dynamics, renewable variability, and energy-storage dispatch.[14,19] In particular, DDPG is appropriate because it is designed for continuous-action control problems rather than purely discrete decisions.[20]

The comparison between the conventional and DDPG-based EMS shows that both strategies maintain DC-bus voltage stability and supply the cold-ironing load. Nevertheless, the DDPG-based EMS provides smoother battery behavior and more adaptive RES coordination. In the base case, the DDPG controller charges the battery smoothly using surplus PV and wind power while keeping the DC bus close to 1,000 V. In the critical case, it responds to sequential PV and wind power reductions by shifting the battery from charging or floating operation to discharging operation without causing significant voltage deviation. In the excess-generation case, it supervises the PV subsystem and activates power-limiting behavior when the battery approaches the upper SOC boundary. This demonstrates that the DDPG controller can manage both shortage and surplus conditions while maintaining system constraints.

The excess-generation case is especially important because it highlights the difference between renewable-energy maximization and safe system operation. In normal renewable operation, PV and wind sources should operate close to their maximum power points to maximize clean-energy utilization. However, when the cold-ironing load is already supplied and the battery is near its upper SOC limit, continuing to extract maximum PV power may lead to overcharge or DC-bus overvoltage. Therefore, PV power limitation becomes necessary. The DDPG-based EMS handles this by coordinating PV power-limiting operation with wind contribution and battery protection. This behavior supports stable standalone RES-based operation without activating the backup grid.

The role of the backup grid interface should therefore be interpreted carefully. In the proposed system, the grid is not designed as a normal power-sharing source. It is included as backup grid support in case of failure of the standalone RES system. In representative simulated cases, the standalone PV–wind–BESS system maintains cold-ironing load supply, so the backup grid is not activated. This is important because the main objective of the system is to supply the ship load from renewable energy and storage, while keeping the grid interface as a reliability layer during failures or critical contingencies. This arrangement is consistent with the aims of reducing dependence on conventional shore power and avoiding the emission-relocation issue associated with a fossil-fuel-dominated electricity supply.[4]

The Alexandria Port real-data case further supports the practical relevance of the proposed approach. By applying realistic meteorological data, the simulation demonstrates that the system can respond to actual variations in solar and wind resources while maintaining the DC-bus voltage close to the reference value. The battery compensates for short-term generation mismatch, while the wind turbine provides additional renewable support when PV generation changes. This confirms the suitability of the PV–wind–BESS configuration for Mediterranean and North African coastal ports, where both solar and wind resources may contribute to renewable-powered shore supply. The use of NASA POWER data also provides a realistic environmental basis for evaluating local renewable availability.[47]

From a port-electrification perspective, the proposed system provides a control-oriented pathway for integrating renewable energy into cold-ironing infrastructure. Cold ironing can reduce local ship emissions during berthing, but its environmental benefit depends strongly on the source of shore-side electricity. Renewable-powered cold ironing can reduce both local port emissions and upstream emissions when compared with fossil-fuel-based supply.[3,4] The use of a common DC bus also supports the integration of converter-based RES, battery storage, and shore-side power-conditioning units. Such architectures are technically attractive because DC systems can simplify the connection of RES and storage elements,[9] while shore-power systems must still satisfy compatibility, safety, and connection requirements for practical port implementation.[35]

Despite these advantages, several limitations should be considered. First, the study is simulation-based, and the proposed EMS has not yet been tested experimentally using hardware-in-the-loop or real-time digital simulation. Second, the battery model focuses mainly on SOC and power exchange, while detailed degradation effects, thermal behavior, and lifetime-cost impacts are not thoroughly investigated. Third, the cold-ironing load is represented as a constant active-power load, which is suitable for evaluating EMS behavior but does not fully represent all possible ship-load dynamics. Fourth, the proposed system is evaluated for a single cold-ironing supply point rather than a complete multi-berth port network. Finally, the DDPG training parameters should be reported using the final MATLAB training script to ensure full reproducibility of the learning process.

Future work should therefore extend the model in several directions. Hardware-in-the-loop validation should be carried out to test the controller under real-time constraints and converter-level dynamics. Battery degradation and temperature-dependent behavior should be included to evaluate long-term operational cost and maintenance requirements. The EMS can also be expanded to include economic optimization, carbon-emission minimization, and berth-scheduling coordination. For larger ports, the model should be extended to multi-berth and multi-ship operation, where several cold-ironing loads may be connected at different times. In addition, safe RL or constraint-aware DDPG methods may be investigated to improve controller reliability before practical deployment.

Overall, the results show that both the conventional rule-based EMS and the proposed DDPG-based EMS can maintain stable operation of the PV–wind–BESS cold-ironing DC microgrid, with the DDPG-based EMS providing enhanced dynamic control performance compared with the conventional approach. The main benefit of the DDPG controller is not only maintaining voltage stability but also providing smoother battery response and more flexible RES supervision under variable operating conditions. Therefore, the proposed comparative framework can support the development of adaptive renewable-powered cold-ironing systems for sustainable port electrification, while keeping backup grid support limited to failure conditions of the standalone RES system.

6. Conclusion

This study presents a comparative evaluation of a conventional rule-based EMS and a DDPG-based EMS for a renewable-powered PV–wind–BESS cold-ironing DC microgrid using a detailed MATLAB/Simulink model. Both controllers successfully maintained stable system operation under normal conditions, renewable-power shortages, excess-generation scenarios, and realistic renewable profiles for Alexandria Port. Notably, the proposed DDPG-based EMS consistently demonstrated smoother and more adaptive control responses than the conventional rule-based approach.

The comparative simulation results showed that the proposed DDPG-based EMS maintained the DC-bus voltage within a narrow operating range of 996.63–1,000 V, demonstrating superior voltage regulation under varying renewable power. In contrast, the conventional rule-based EMS exhibited larger transient voltage excursions during the same operating conditions. Overall, the proposed DDPG-based controller reduced the maximum DC-bus voltage deviation by 30%–35%, while providing smoother battery charging and discharging behavior and more effective coordination between the PV generation, wind generation, and BESS. These improvements enabled the standalone renewable energy system to satisfy the cold-ironing load throughout the investigated scenarios without requiring emergency grid support.

The Alexandria Port case study demonstrates the applicability of the proposed methodology under representative Mediterranean and North African RES conditions. Rather than proposing a region-specific control strategy, the study illustrates how intelligent energy management can be effectively evaluated using realistic local RES profiles and operational constraints. Consequently, the proposed framework can be adapted to other cold-ironing installations by incorporating the specific RES characteristics, load requirements, and infrastructure conditions.

Despite its improved dynamic performance, the proposed DDPG-based EMS requires offline training, greater computational complexity, and more careful parameter tuning compared with a conventional rule-based controller. Furthermore, the present work is limited to simulation-based validation using MATLAB/Simulink. Future work will therefore focus on hardware-in-the-loop and laboratory-scale experimental validation, battery degradation modeling, variable ship-load profiles, multi-berth cold-ironing operation, and techno-economic assessment to further evaluate the practical deployment of the proposed energy management strategy.

Overall, this work demonstrates that the proposed DDPG-based EMS provides a more adaptive and effective energy management strategy than the conventional rule-based EMS for renewable-powered cold-ironing DC microgrids. By improving DC-bus voltage regulation, battery management, and RES coordination under dynamic operating conditions, the proposed approach represents a promising intelligent control solution for future sustainable port electrification systems.

Acknowledgments

None.

Funding

None.

Conflict of interest

The authors declare that they have no conflict of interest.

Author contributions

Conceptualization: Mohab M. Eweda, Ahmed K. Abdelsalam
Formal analysis: Mohab M. Eweda
Investigation: Mohab M. Eweda
Methodology: Mohab M. Eweda, Rana M. Ahmed, Mona I. Abdelkader
Writing – original draft: Mohab M. Eweda
Writing – review & editing: Rana M. Ahmed, Mona I. Abdelkader, Ahmed K. Abdelsalam

Availability of data

The data supporting the findings of this study are available from the corresponding author upon reasonable request.

AI tools statement

All authors confirm that no AI tools were used in the preparation of this manuscript.

References

1. Canepa M, Ballini F, Dalaklis D, Frugone G, Sciutto D. Cold Ironing: Socio-Economic Analysis in the Port of Genoa. *Logistics*. 2023;7(2):28.

   https://doi.org/10.3390/LOGISTICS7020028

2. Spengler T, Tovar B. Potential of cold-ironing for the reduction of externalities from in-port shipping emissions: The state-owned Spanish port system case. *J Environ Manage*. 2021;279:111807.

   https://doi.org/10.1016/J.JENVMAN.2020.111807

3. Piccoli T, Fermeglia M, Bosich D, Bevilacqua P, Sulligoi G. Environmental Assessment and Regulatory Aspects of Cold Ironing Planning for a Maritime Route in the Adriatic Sea. *Energies*. 2021;14(18):5836.

   https://doi.org/10.3390/EN14185836

4. Yuksel O, Bayraktar M, Seyhan A. Environmental and economic analysis of cold ironing using renewable hybrid systems. *Clean Technol Environ Policy*. 2025;27(8):3489-3517.

   https://doi.org/10.1007/S10098-024-03065-W

5. Rolan A, Manteca P, Oktar R, Siano P. Integration of Cold Ironing and Renewable Sources in the Barcelona Smart Port. *IEEE Trans Ind Appl*. 2019;55(6):7198-7206.

   https://doi.org/10.1109/TIA.2019.2910781

6. Ghedamsi A, Mabrouk A, Bouaicha H, Belhadj J. PV power plant for Cold Ironing at the Goulette port. In: *2022 IEEE International Conference on Electrical Sciences and Technologies in Maghreb (CISTEM)*. New York, NY: IEEE; 2022:1-6.

   https://doi.org/10.1109/CISTEM55808.2022.10044041

7. Kumar J, Parthasarathy C, Västi M, Laaksonen H, Shafie-Khah M, Kauhaniemi K. Sizing and Allocation of Battery Energy Storage Systems in Åland Islands for Large-Scale Integration of Renewables and Electric Ferry Charging Stations. *Energies*. 2020;13(2):317.

   https://doi.org/10.3390/en13020317

8. Johnson SC, Papageorgiou DJ, Harper MR, Rhodes JD, Hanson K, Webber ME. The economic and reliability impacts of grid-scale storage in a high penetration renewable energy system. *Adv Appl Energy*. 2021;3:100052.

   https://doi.org/10.1016/j.adapen.2021.100052

9. Prenc R, Cuculić A, Baumgartner I. Advantages of using a DC power system on board ship. *J Marit Transp Sci*. 2016;52(1):83-97.

   https://doi.org/10.18048/2016.52.05

10. Alabdullah MH, Abido MA. Microgrid energy management using deep Q-network reinforcement learning. *Alex Eng J*. 2022;61(11):9069-9078.

    https://doi.org/10.1016/J.AEJ.2022.02.042

11. Ji Y, Wang J, Xu J, Fang X, Zhang H. Real-Time Energy Management of a Microgrid Using Deep Reinforcement Learning. *Energies*. 2019;12(12):2291.

    https://doi.org/10.3390/EN12122291

12. Guo C, Wang X, Zheng Y, Zhang F. Real-time optimal energy management of microgrid with uncertainties based on deep reinforcement learning. *Energy*. 2022;238:121873.

    https://doi.org/10.1016/J.ENERGY.2021.121873

13. Foruzan E, Soh LK, Asgarpoor S. Reinforcement Learning Approach for Optimal Distributed Energy Management in a Microgrid. *IEEE Trans Power Syst*. 2018;33(5):5749-5758.

    https://doi.org/10.1109/TPWRS.2018.2823641

14. Barbalho PIN, Moraes AL, Lacerda VA, Barra PHA, Fernandes RAS, Coury DV. Reinforcement Learning Solutions for Microgrid Control and Management: A Survey. *IEEE Access*. 2025;13:39782-39799.

    https://doi.org/10.1109/ACCESS.2025.3546578

15. Muriithi G, Chowdhury S. Optimal Energy Management of a Grid-Tied Solar PV-Battery Microgrid: A Reinforcement Learning Approach. *Energies*. 2021;14(9):2700.

    https://doi.org/10.3390/EN14092700

16. Du Y, Li F. Intelligent Multi-Microgrid Energy Management Based on Deep Neural Network and Model-Free Reinforcement Learning. *IEEE Trans Smart Grid*. 2020;11:1066-1076.

    https://doi.org/10.1109/TSG.2019.2930299

17. Hosseini E, Horrillo-Quintero P, Carrasco-Gonzalez D, *et al*. Reinforcement learning-based energy management system for lithium-ion battery storage in multilevel microgrid. *J Energy Storage*. 2025;109:115114.

    https://doi.org/10.1016/J.EST.2024.115114

18. Upadhyay S, Ahmed I, Mihet-Popa L. Energy

Management System for an Industrial Microgrid Using Optimization Algorithms-Based Reinforcement Learning Technique. *Energies*. 2024;17(16):3898.

https://doi.org/10.3390/EN17163898

19. Kumar K, Kwon S, Bae S. Deep reinforcement learning-based control strategy for integration of a hybrid energy storage system in microgrids. *J Energy Storage*. 2025;108:114936.

    https://doi.org/10.1016/j.est.2024.114936

20. Talab OA, Avci I. Energy Management in Microgrids Using Model-Free Deep Reinforcement Learning Approach. *IEEE Access*. 2025;13:5871-5891.

    https://doi.org/10.1109/ACCESS.2025.3525843

21. Villalva MG, Gazoli JR, Ruppert Filho E. Comprehensive approach to modeling and simulation of photovoltaic arrays. *IEEE Trans Power Electron*. 2009;24(5):1198-1208.

    https://doi.org/10.1109/TPEL.2009.2013862

22. Tian H, Mancilla-F David, Ellis K, Muljadi E, Jenkins P. A cell-to-module-to-array detailed model for photovoltaic panels. *Sol Energy*. 2012;86(9):2695-2706.

    https://doi.org/10.1016/J.SOLENER.2012.06.004

23. Qi C, Ming Z. Photovoltaic Module Simulink Model for a Stand-alone PV System. *Phys Procedia*. 2012;24:94-100.

    https://doi.org/10.1016/J.PHPRO.2012.02.015

24. Tsai HL, Tu CS, Su YJ. Development of Generalized Photovoltaic Model Using MATLAB/SIMULINK. In: *Proceedings of the World Congress on Engineering and Computer Science 2008*. Hong Kong: International Association of Engineers; 2008. Accessed May 16, 2026. https://www.iaeng.org/publication/WCECS2008/WCECS2008_pp846-851.pdf

25. Qin L, Lu X. Matlab/Simulink-Based Research on Maximum Power Point Tracking of Photovoltaic Generation. *Phys Procedia*. 2012;24:10-18.

    https://doi.org/10.1016/J.PHPRO.2012.02.003

26. Hart DW. *Power Electronics*. New York, NY: The McGraw-Hill Companies, Inc; 2010.

27. Ahmed R, Naaman A, M'Sirdi NK, Abdelsalam AK, Dessouky YG. Sensorless MPPT technique for PMSG micro wind turbines based on state-flow. In: *2014 International Conference on Renewable Energies for Developing Countries*. New York, NY: IEEE; 2014:161-166.

    https://doi.org/10.1109/REDEC.2014.7038550

28. Al-Nhoud O, Al-Smairan M. Assessment of Wind Energy Potential as a Power Generation Source in the Azraq South, Northeast Badia, Jordan. *Mod Mech Eng*. 2015;5(3):87-96.

    https://doi.org/10.4236/MME.2015.53008

29. Koutroulis E, Kalaitzakis K. Design of a maximum power tracking system for wind-energy-conversion applications. *IEEE Trans Ind Electron*. 2006;53(2):486-494.

    https://doi.org/10.1109/TIE.2006.870658

30. Buticchi G, Lorenzani E, Immovilli F, Bianchini C. Active rectifier with integrated system control for microwind power systems. *IEEE Trans Sustain Energy*. 2015;6(1):60-69.

    https://doi.org/10.1109/TSTE.2014.2356335

31. MathWorks. Battery: Behavioral battery model. Simscape Battery Documentation. Accessed May 16, 2026. https://www.mathworks.com/help/simscape-battery/ref/battery.html

32. MathWorks. Battery state of charge. MathWorks. Accessed May 16, 2026. https://www.mathworks.com/discovery/battery-state-of-charge.html

33. Hauke B. Basic Calculation of a Boost Converter's Power Stage. Application report SLVA372D. Rev November 2022. Dallas, TX: Texas Instruments; 2022. Accessed May 16, 2026. https://www.ti.com/lit/an/slva372d/slva372d.pdf

34. Lee J. Basic Calculation of a Buck Converter's Power Stage. Application Note AN041. December 2015. Taipei, Taiwan: Richtek Technology Corporation; 2015. Accessed May 16, 2026. https://www.richtek.com/Design%20Support/Technical%20Document/AN041

35. International Electrotechnical Commission, Institute of Electrical and Electronics Engineers. IEC/IEEE 80005-1:2019. Utility connections in port–Part 1: High voltage shore connection (HVSC) systems—General requirements. Published March 2019. Accessed May 17, 2026. https://www.iso.org/standard/64717.html

36. Bird J. *Electrical Circuit Theory and Technology*. 6th ed. Abingdon, UK: Routledge; 2017.

    https://doi.org/10.4324/9781315561929

37. Jamal S, Pasupuleti J, Ekanayake J. A rule-based energy management system for hybrid renewable energy sources with battery bank optimized by genetic algorithm optimization. *Sci Rep*. 2024;14(1):4865.

    https://doi.org/10.1038/s41598-024-54333-0

38. Ahmed R. *Energy management and control for hybrid renewable energy sources in rural area*. Dissertation. Aix-Marseille, France: Aix-Marseille University; 2015.

    https://doi.org/10.70675/DA0CCD0BZEBC9Z4FECZ94A3Z6F292EA669F6

39. Åström KJ, Murray RM. *Feedback Systems:*

An Introduction for Scientists and Engineers. Princeton, NJ: Princeton University Press; 2010.

40. Ogata K. *Modern Control Engineering*. 5th ed. Upper Saddle River, NJ: Prentice Hall; 2002.
41. MathWorks. Rate Limiter: Limit rate of change of signal. Simulink Documentation. Accessed May 17, 2026. https://www.mathworks.com/help/simulink/slref/ratelimiter.html
42. Sutton RS, Barto AG. *Reinforcement Learning: An Introduction*. 2nd ed. Cambridge, MA: Bradford Books; 2018.
43. Silver D, Lever G, Heess N, Degris T, Wierstra D, Riedmiller M. Deterministic Policy Gradient Algorithms. *Proceedings of the 31st International Conference on Machine Learning Research*. 2014;32(1):387-395. https://proceedings.mlr.press/v32/silver14.html
44. Lillicrap TP, Hunt JJ, Pritzel A, *et al.* Continuous control with deep reinforcement learning. Preprint posted online September 9, 2015. arXiv.

    https://doi.org/10.48550/arXiv.1509.02971
45. Wu H, Locment F, Sechilariu M. Experimental Implementation of a Flexible PV Power Control Mechanism in a DC Microgrid. *Energies*. 2019;12(7):1233.

    https://doi.org/10.3390/EN12071233
46. Goh HH, Huang Y, Lim CS, *et al.* An Assessment of Multistage Reward Function Design for Deep Reinforcement Learning-Based Microgrid Energy Management. *IEEE Trans Smart Grid*. 2022;13(6):4300-4311.

    https://doi.org/10.1109/TSG.2022.3179567
47. National Aeronautics and Space Administration. NASA POWER Data Access Viewer. NASA Prediction of Worldwide Energy Resource (POWER). Accessed August 7, 2026. https://power.larc.nasa.gov/data-access-viewer/

Mohab M. Eweda received the B.Sc. and M.Sc. degrees in Electrical and Control Engineering from the Arab Academy for Science, Technology and Maritime Transport (AASTMT), Egypt. He is currently a Lecturer at the Institute of Maritime Upgrading Studies (IMUS) at Arab Academy for Science, Technology and Maritime Transport (AASTMT) and is pursuing a Ph.D. in Electrical Engineering at AASTMT. His research interests include renewable energy systems, hybrid microgrids, intelligent energy management systems, deep reinforcement learning, power electronics, and cold-ironing systems for sustainable port electrification.
https://orcid.org/0009-0001-6633-7840

Rana M. Ahmed received the Ph.D. degree in Electrical Engineering and is currently an Associate Professor with the College of Engineering and Technology, AASTMT, Egypt. Her research interests include renewable energy systems, power electronics, smart grids, electric drives, microgrids, and intelligent energy management systems.
https://orcid.org/0000-0002-2840-7975

Mona I. Abdelkader received the Ph.D. degree in Electrical Engineering and is currently an Associate Professor with the College of Engineering and Technology, AASTMT, Egypt. Her research interests include renewable energy integration, electrical power systems, power electronics, optimization techniques, and sustainable energy technologies.
https://orcid.org/0009-0009-3541-2834

Ahmed K. Abdelsalam received the Ph.D. degree in Electrical Engineering and is currently a Professor with the College of Engineering and Technology, AASTMT, Egypt. His research interests include power electronics, electrical machines, renewable energy systems, intelligent control, and smart grid technologies.
https://orcid.org/0000-0003-3157-2274